Middle Atmospheric Traveling Waves Forced by Latent and Convective Heating

ELISA MANZINI*

Atmospheric and Oceanic Sciences Program, Princeton University, Princeton, New Jersey

KEVIN HAMILTON

Geophysical Fluid Dynamics Laboratory/NOAA, Princeton University, Princeton, New Jersey

(Manuscript received 6 July 1992, in final form 22 October 1992)

ABSTRACT

The excitation and propagation of equatorial planetary waves and inertia–gravity waves were studied by comparing simulations from the comprehensive GFDL troposphere–stratosphere–mesosphere SKYHI general circulation model (GCM) and from a linear primitive equation model with the same domain and numerical resolution. The basic state of the linear model is time dependent and is derived from the mean zonal wind and temperature obtained from a simulation with the full SKYHI model. The latent and convective heating fields of this SKYHI integration are used as the forcing for the linear model in a parallel simulation.

The wavelength and frequency characteristics of the prominent vertically propagating equatorial Kelvin and Rossby–gravity waves are remarkably similar in the linear model and in SKYHI. Amplitudes are also similar in the lower stratosphere, indicating that the latent and convective heating is the dominant mechanism producing equatorial wave activity in the GCM. The amplitude of these waves in the upper stratosphere and mesosphere is larger in the linear model than in SKYHI. Given that the linear and SKYHI models have comparable radiative damping and horizontal subgrid scale diffusion, it appears that the wave amplitudes in SKYHI are limited by some nonlinear saturation, possibly involving the subgrid-scale vertical mixing.

At low latitudes the linear model reproduces the flux of upward-propagating inertia–gravity waves seen in the full model. The results also show that a significant fraction of the inertia–gravity wave activity found in the midlatitude mesosphere of the SKYHI model can be accounted for by tropical convective heating.

The global-scale Rossby normal modes seen in observations were also identified in the analyses of westward-propagating planetary waves in both models. They are of realistic amplitude in the SKYHI simulation but are much weaker in the linear model. Thus, it appears that latent and convective heating is not the main source of excitation for the Rossby normal modes.

1. Introduction

Middle atmospheric meteorology is largely concerned with understanding various types of traveling stratospheric and mesospheric waves. The first-order behavior of such waves over much of the atmosphere is reasonably described by linear theory. The analysis of both observational data and general circulation model (GCM) simulations in light of simple linear solutions has allowed the identification of particular features of the middle atmospheric circulation as Rossby normal modes, vertically propagating equatorial waves, and vertically propagating inertia–gravity waves (e.g., Andrews et al. 1987). The prime energy source for all these waves is presumably in the troposphere, but the detailed understanding of the excitation mechanisms responsible for the observed wave spectrum is still a matter of active investigation.

Considerable work has been done on the possible excitation mechanisms for the large-scale equatorial waves. Mak (1969) proposed that tropical disturbances might be driven by midlatitude forcing at the poleward boundaries of the tropical region. He demonstrated that in a two-layer model, westward Rossby–gravity waves similar to the observed Yanai–Maruyama wave (Yanai and Maruyama 1966; Wallace 1973) can indeed be generated by this mechanism. This excitation should be most effective near the solstices, but such a seasonal dependence is not supported by observations of the amplitude of atmospheric Rossby–gravity waves (Hendon and Liebmann 1991). Mak's mechanism is also likely to be quite ineffective in forcing Kelvin waves (which have small meridional velocity).

There have been two different theoretical approaches to understanding the possible role of latent heating in forcing equatorial planetary waves. In the wave–CISK

* Current affiliation: Max-Planck-Institut for Meteorology, Bundesstrasse 55, W 2000 Hamburg 13, Germany.

Corresponding author address: Dr. Kevin Hamilton, Princeton University, GFDL/NOAA, Atmospheric and Ocean Sciences Program, P.O. Box 308, Princeton, NJ 08542.

(convective instability of the second kind) theories, the mutual interaction of moisture convergence by the waves and latent heat release leads to an instability (e.g., Hayashi 1970). The presumption then is that the fastest growing linear modes will dominate both the convective heating and the wave motions in the fully developed flow. Observational evidence of spectral peaks in tropical convection has been found only for frequencies corresponding to the Yanai–Maruyama wave (Nitta 1970; Hendon and Liebmann 1991) but not for any of the prominent Kelvin waves.

In the other approach (Holton 1973; Salby and Garcia 1987; Garcia and Salby 1987), a random heating is specified in the tropical troposphere and the dynamical response is computed using linear theory. The principal result of these studies is that the vertical structure of the specified heating plays a crucial role in determining the dominant vertical wavelength (and hence horizontal phase speed) of the response. Thus, even if the forcing has no preferred frequency, the wave response in the stratosphere may be concentrated over a limited band of frequencies.

Hayashi and Golder (1978) attempted to separate the effects of various forcing mechanisms for equatorial waves by performing a series of controlled experiments with a comprehensive GCM of the troposphere and lower stratosphere. They compared a simulation made with the full model with simulations made with simplified versions, one without a hydrological cycle and one with eddies arbitrarily suppressed poleward of 30°. The removal of the midlatitude eddies significantly reduces the amplitude of the simulated Rossby–gravity waves but has little effect on the Kelvin waves. Elimination of the hydrological cycle results in a simulation in which both the stratospheric Kelvin and Rossby–gravity waves are virtually absent. They concluded that latent heat release is by far the dominant excitation mechanism for the Kelvin waves, while the Rossby–gravity waves are forced by a combination of latent heating and propagation of disturbances from the extratropics. Unfortunately such controlled experiments cannot be performed in a straightforward way, since both the elimination of midlatitude eddies and the removal of the hydrological cycle produce very unrealistic simulations. Hayashi and Golder (1978) dealt with this problem by including in their model equations an arbitrary relaxation to prescribed mean flows and vertical temperature gradients.

In addition to the equatorial planetary waves, the tropical atmospheric circulation may include higher-frequency and smaller-scale vertically propagating disturbances. Variations in the extratropical mesospheric wind having periods of minutes to hours have long been interpreted as evidence for vertically propagating inertia–gravity waves (e.g., Hines 1960). In the tropics, where the Coriolis parameter is small, such waves can have longer periods. In a recent study, Hamilton and Mahlman (1988) found that gravity waves with periods extending from hours to days and with horizontal scales of several hundred to some thousands of kilometers play an important role in the tropical circulation of the middle atmosphere of the GFDL SKYHI troposphere–stratosphere–mesosphere GCM.

Some attention has been devoted to orography, shear instability, and frontal collapse as possible excitation mechanisms for vertically propagating gravity waves (e.g., Fritts 1984; Nastrom and Fritts 1992; Fritts and Nastrom 1992). These forcings, however, are likely to be more significant in the extratropics than in low latitudes where the tropospheric mean winds are weak. Cumulus convection provides the most obvious excitation for tropical gravity waves.

A number of recent studies have raised the possibility that a significant tropical heating source may exist for gravity waves in the extratropical upper stratosphere and mesosphere. An examination of the total Eliassen–Palm flux in a SKYHI model simulation led Miyahara et al. (1986) to suggest that the gravity waves found in the midlatitude mesosphere might have their origins in the tropospheric low latitudes. Detailed statistical analysis of radar observations at Adelaide (35°S, 138°E) by Vincent and Fritts (1987) and of rocketsonde observations at Woomera (31°S, 136°E) by Eckermann and Vincent (1989) have revealed the preferred horizontal orientation of mesospheric wind fluctuations. The authors interpreted this as indicating a dominant direction for the propagation of inertia–gravity waves. During the summer season, a southeastward propagation was inferred. Therefore, the authors speculated that the sources of the gravity waves might be located in the equatorial troposphere north of Australia. Similar results from observations at a number of Northern Hemisphere extratropical rocketsonde stations have been obtained recently by Hamilton (1991).

Atmospheric Rossby normal-mode oscillations (such as the familiar "2 day," "5 day," and "16 day" waves) are quite prominent features of the mesospheric and upper-stratospheric circulation (e.g., Salby 1984). Some research has been done on possible excitation mechanisms for Rossby normal modes in the atmosphere. Garcia and Geisler (1981) found that these modes are excited by variations in the strength of the mean flow over large-scale topography in a very simple model. From the simple diagnostic study of Hamilton (1987), it appears that the latent heat release makes at least some contribution to the excitation of the Rossby normal modes in a full general circulation model. Hayashi and Golder (1983) speculated that nonlinear wave–wave interactions in the troposphere may play an important role in forcing these normal modes. It is fair to say, however, that at present nothing conclusive can be said about the significance of any of these mechanisms.

The present paper examines the role of convective heating in generating equatorial waves, tropical and

extratropical gravity waves, and global Rossby normal modes. The investigation makes use of the availability of the GFDL SKYHI GCM, which is known to produce a simulation with a rich (and in some respects realistic) spectrum of middle atmospheric waves (e.g., Hayashi et al. 1984; Miyahara et al. 1986; Hamilton and Mahlman 1988; Hamilton 1988; Hayashi et al. 1989). In the work described here, the traveling waves in a 78-day SKYHI integration are examined in detail and compared with those appearing in a parallel integration of a linearized version of the model. The linear model is forced only by the time series of latent and convective heating taken from the full model integration. This simple approach will be shown to lead to some quite unambiguous conclusions concerning the significance of convective heating for the various types of middle atmospheric waves. The detailed analysis of the SKYHI simulation itself has also produced interesting new results, most notably in the demonstration that the model has a rather realistic spectrum of atmospheric Rossby normal modes.

The research reported here is described in more detail in Manzini (1992), hereafter referred to as M92. The documentation for many of the results discussed in sections 4–6 can be found in M92.

A brief description of the SKYHI model and some results obtained from the control integration are given in section 2. Section 3 describes the basic features of the linear model integration. Section 4 discusses the results obtained for global-scale vertically propagating equatorial waves. Section 5 presents the results for higher-frequency motions, which are identified here as inertia–gravity waves. Section 6 discusses those aspects of the results that relate to Rossby normal modes. The conclusions are summarized in section 7.

2. The SKYHI Model

a. *Model formulation*

SKYHI is a comprehensive GCM designed to simulate the evolution of the general circulation of the troposphere, stratosphere, and mesosphere (Fels et al. 1980). In SKYHI, the full nonlinear primitive equations are discretized on a latitude–longitude grid by means of the box method (Kurihara and Holloway 1967). At high latitudes a Fourier filter is applied to enforce an approximately uniform longitudinal scale. An explicit leapfrog scheme, combined with a time filter with the Euler backward scheme applied once every 24 time steps, is used to integrate the prediction equations. The model uses a hybrid vertical coordinate system, which is terrain following near the ground and purely isobaric above 321 mb. The vertical domain of SKYHI ranges from the surface to the top prediction level at 0.0096 mb (about 80 km) and is discretized on 40 levels. The vertical spacing between levels slowly increases with height and is about 2 km in the stratosphere. At the top level a linear damping with a coefficient value of $(10\ 800\ \text{s})^{-1}$ is applied to all deviations from the zonal mean. This acts as a crude sponge layer to reduce spurious reflections. A realistic topography and a zonally symmetric distribution of clouds are prescribed, along with a realistic seasonally varying ocean surface temperature. The solar diurnal cycle has not been included.

Of particular interest to the present work are the precipitation and convection parameterizations. The parameterizations used in SKYHI consist of moist and dry convective adjustment as well as the production of stable rain. The saturation criterion in both the stable rain and moist convection schemes is taken to be 85% of the saturation mixing ratio computed using grid-scale temperatures. The total temperature change that occurs in applying the precipitation and convection parameterizations will be referred to as the SKYHI "thermal forcing" when it is used in the linear model experiments described later.

The SKYHI model employs a modification of the nonlinear Smagorinsky horizontal diffusion as described in Andrews et al. (1983), for the temperature and horizontal wind fields. The vertical mixing consists of a (very small) molecular diffusion and a subgrid-scale turbulence parameterization that depends on the Richardson number (nonzero only when the Richardson number drops below 1). A standard surface drag formulation (with a Monin–Obukhov scheme to determine the drag coefficient) is employed.

During the last decade, integrations of several versions of SKYHI with different horizontal resolution have been analyzed. Hayashi et al. (1984) examined a simulation obtained with $5° \times 6°$ latitude–longitude resolution. They found evidence for prominent equatorial Kelvin waves with scales and frequencies comparable to the observed "slow" (Wallace and Kousky 1966), "fast" (Hirota 1978), and "ultrafast" (Salby et al. 1984) waves seen in observations. Simulations with the $3° \times 3.6°$ and the $1° \times 1.2°$ versions of the model are discussed in Miyahara et al. (1986) and Hayashi et al. (1989). These analyses showed the presence in both the midlatitudes and the tropics of upward-propagating high-frequency oscillations identified as inertia–gravity waves. The frequency–wavenumber spectrum of the inertia–gravity waves broadens as the resolution is increased. Eastward- and westward-moving gravity waves are selectively filtered by the stratospheric winds in accord with the predictions of simple theoretical models (e.g., Lindzen 1981). Miyahara et al. (1986) found that the zonal momentum flux convergence due to the gravity waves contributes substantially to the total wave driving of the mean flow in the mesosphere.

b. *The present simulation*

The present study focuses on a 78-day period, 1 April–16 June, from the third year of a long control

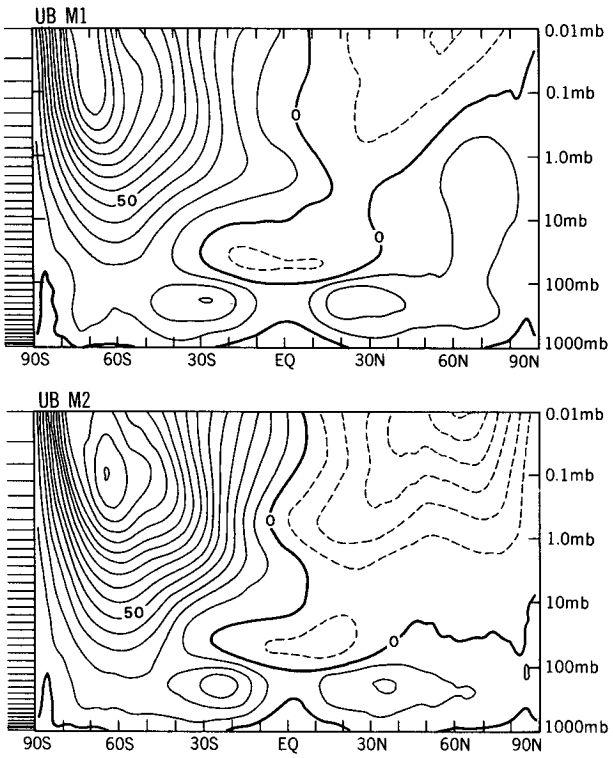

FIG. 1. Meridional section of the zonal-mean zonal wind from the SKYHI simulation averaged over (top) the M1 period and (bottom) the M2 period. Contour interval: 10 m s^{-1}. Easterly winds are denoted by dashed contours.

integration of the 3° × 3.6° SKYHI model. The analysis will concentrate on the last 60 days of this period, which for convenience are divided into two 30-day intervals denoted by M1 (18 April–17 May) and M2 (18 May–16 June).

Figure 1 shows the zonal-mean zonal wind averaged over the M1 and M2 periods. The overall simulation is reasonably good, although the Southern Hemisphere mesospheric jet is much stronger than observed. Near the mesopause the summertime easterly jet is also somewhat too strong during the M2 period. The stratopause semiannual oscillation in the equatorial zonal wind is clearly present (note the evolution near 1 mb from mean westerly winds during the M1 period to mean easterly winds during the M2 period). As in other GCM simulations, this model produces virtually no quasi-biennial oscillation in the lower stratosphere, however.

Figure 2 shows the mean precipitation averaged over 1 April–30 June of this third year of simulation. The distribution of the precipitation seen here has generally good agreement with observations (e.g., Legates and Willimott 1990; Taylor 1973). There are some significant deficiencies, however. In particular, the simulated precipitation is much too light over northern India. In the equatorial west Pacific the model precipitation shows a single equatorial maximum, rather than the two off-equatorial maxima seen in observations. In the observations (Legates and Willmott 1990), there is also a separate equatorial maximum in rainfall east of the date line (presumably associated with El Niño conditions) that is not found in Fig. 2. These problems are not confined to the three-month period covered in Fig. 2, but also appear in the long-term mean SKYHI control climatology.

3. The linear model

a. Basic formulation

The simple model developed for this study was designed to solve the primitive equations in isobaric coordinates linearized about a zonally symmetric basic

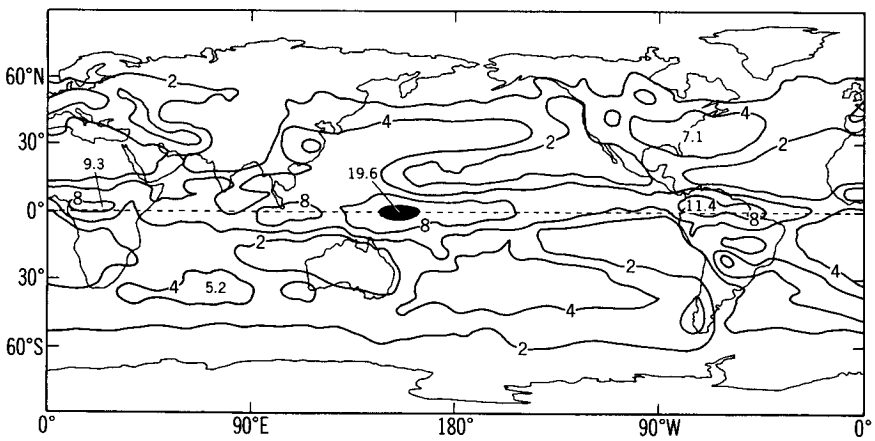

FIG. 2. Mean precipitation for April–May–June for the SKYHI simulation. The contour value doubles at each interval, starting from 2 mm day^{-1}. The region with precipitation greater than 16 mm day^{-1} is heavily shaded.

state. The model domain is global and extends to 0.0096 mb. The 40 vertical levels employed are identical to those at a SKYHI grid point with surface pressure of 1013.25 mb. No orography is included in the linear model and the geopotential height of the lowest model level is a prognostic variable. The solution is represented by a spectral expansion in the zonal direction. Linearized versions of the SKYHI finite-difference approximations are employed to represent the vertical and meridional derivatives. The meridional resolution is 3°, and only zonal wavenumber 1 is integrated from pole to pole; for all other zonal wavenumbers a wall is imposed at the latitude where the Fourier filter is used in SKYHI. As in SKYHI, the linear model is integrated with explicit leapfrog time differencing. The linear model employed a weak Robert filter applied at each time step (rather than the intermittent application of time filtering in the full SKYHI model).

The linear model includes dissipation in the momentum and thermodynamic equations. In particular, a Newtonian cooling designed to roughly approximate the radiative transfer term in the full SKYHI model was employed. The coefficient was taken from the Fels (1982) scale-dependent parameterization assuming a vertical wavelength of 15 km (the mean temperature profile needed in Fels formula was taken as the "tropical standard" from Fels 1986). A ∇^2 diffusion of both temperature and momentum with coefficient $K_H = 1.8 \times 10^5$ m^2 s^{-1} was also employed. In M92 there is a comparison of this value with spatial averages of values of the (deformation dependent) K_H in the full SKYHI simulation. The K_H used in the linear model is roughly a factor of 2–3 larger than the mean values in SKYHI. Just as in the full SKYHI model, an arbitrary linear damping of eddy fields is imposed at the top level of the linear model. No surface drag is included in the linear model.

b. *Suppression of baroclinic instability*

When the linear model is integrated with forcing in the thermodynamic equation and basic state taken from the SKYHI control, exponentially growing baroclinic waves appear. These disturbances are strongest in the midlatitude lower troposphere, but after several weeks of integration they dominate the solution almost everywhere. A trial and error approach was used to arrive at the minimum modification to the model that successfully suppressed the baroclinic instability. The solution ultimately adopted was to (i) eliminate the mean state baroclinicity poleward of 43.5°S and 40.5°N and between the ground and 321 mb, (ii) include a linear damping in narrow surface layers extending over the lowest three levels (1003.7 to 922.2 mb) and poleward of 22.5° latitude, and (iii) include a linear damping in polar sponge regions extending the full depth of the model poleward of 73.5° latitude. To accomplish (i), the mean state temperature at all points poleward of 40.5°N and all levels below 321 mb was set to the temperature at the same level at 40.5°N. The mean zonal wind at levels below 321 mb and points poleward of 40.5°N was set to the value at 321 mb at the same latitude. A similar procedure was adopted for the Southern Hemisphere poleward of 43.5°S. Further details are given in M92.

c. *The parallel SKYHI and linear model integrations*

During the SKYHI integration from 1 April to 16 June, the hourly mean values of wind, temperature, surface pressure, and subgrid-scale "thermal forcing" were achieved.

The linear model was integrated from zero initial conditions for the same 78 days using a time step of 225 s (changed to 112.5 s for the last 30 days). The eddy thermal forcing and zonal mean state were taken from the SKYHI integration and were updated every hour throughout the linear model run. In order to focus on the effects of tropospheric wave excitation, the thermal forcing was set equal to zero above 103 mb (thus eliminating any contribution from activation of the dry convective adjustment in the middle atmosphere). Before insertion into the linear model, the SKYHI thermal forcing at each grid point was also multiplied by the ratio of the simulated surface pressure to the standard surface pressure (1013.25 mb). This correction (normally only a few percent) was a crude attempt to account for the use of a constant mean surface pressure in the linear model.

In order to keep the volume of data archived within practical bounds, a number of simplifications were adopted. While all fields were archived at all latitudes and pressure levels equatorward of 43.5°, only the zonal mean fields in SKYHI were archived poleward of 43.5°. This allowed a global mean state to be specified for the linear model, but meant that the thermal forcing was set to zero poleward of 43.5°. This is a reasonable simplification, given the present focus on convective heating and given the considerable modification that had to be imposed on the high-latitude mean state. Instantaneous values of the linear model fields equatorward of 43.5° were saved every hour. The zonal resolution of the linear model was restricted to wavenumbers 1–24 (i.e., down to wavelengths approximately four times the zonal grid spacing in SKYHI). Earlier studies with the 3° × 3.6° SKYHI model (e.g., Hamilton and Mahlman 1988) suggest that less than 10% of the vertical eddy momentum flux in the middle atmosphere resides in the portion of the spectrum with wavelengths less than four times the grid spacing (this part of the spectrum is also poorly represented by the finite-difference numerical scheme of the SKYHI model).

d. *Analysis applied to the results*

The hourly fields from both the SKYHI and linear model integrations were sampled every four hours and

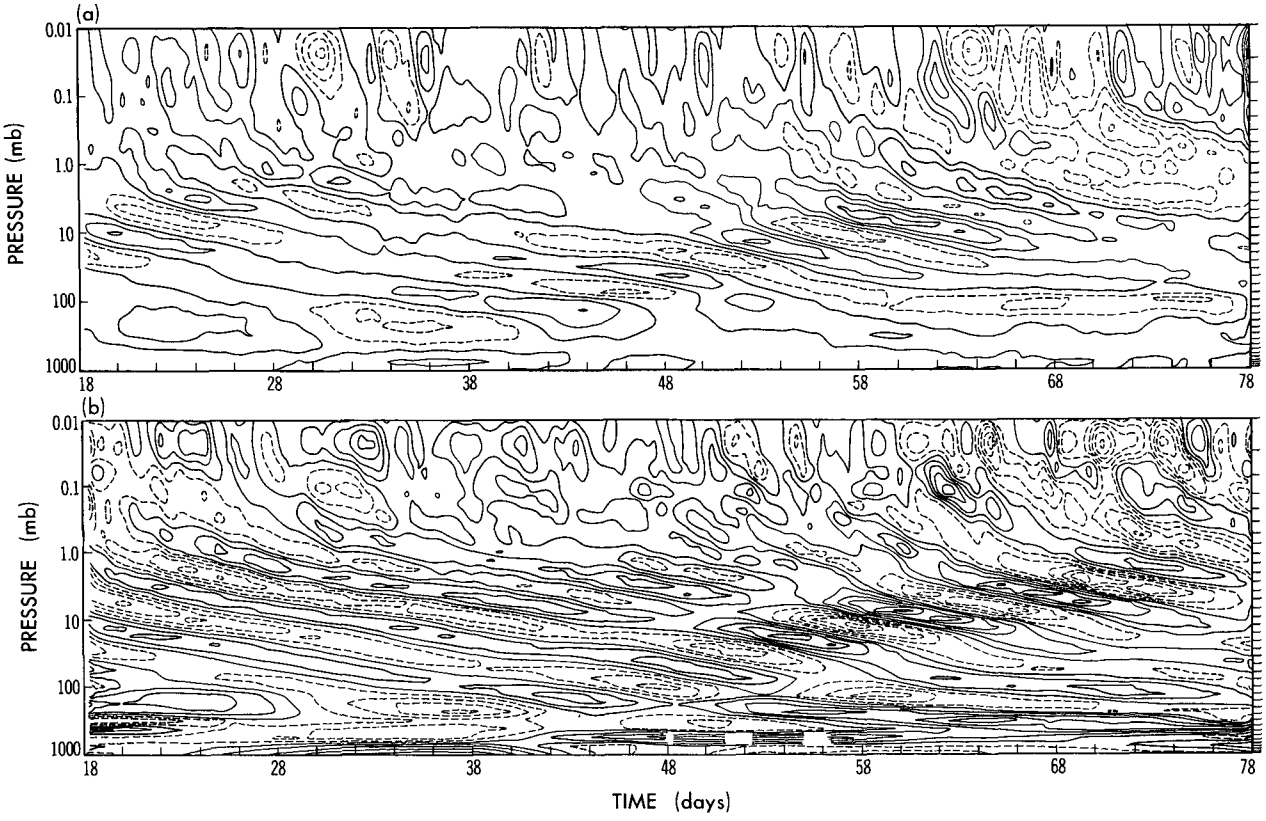

FIG. 3. Time–height section of the equatorial zonal wind for eastward-propagating wavenumber 1 at 0° longitude over the M1 and M2 periods. (a) SKYHI and (b) linear model. Contour interval: 2 m s^{-1}. Dashed contours indicate easterly winds. The tick marks on the vertical axis represent the locations of model levels.

then analyzed into westward- and eastward-propagating components using space–time Fourier analysis (Hayashi 1971). This was done separately for the M1 and M2 periods. In addition, for the zonal wavenumbers 1–4, a similar analysis into westward and eastward components was carried out using 8-hourly data (means of two 4-hourly snapshots) for the 60-day period 18 April–16 June (linear model) and for the full 78-day period 1 April–16 June (SKYHI). Some comparisons of results using hourly data and the 4- or 8-hourly data showed only small differences. In all cases, the space–time Fourier analysis was performed at all levels and all latitudes from 43.5°S to 43.5°N. The zero frequency eddy component of the simulation was not analyzed and is excluded from all results presented in this paper.

4. Large-scale equatorial waves

a. Results for eastward-propagating wavenumbers 1 and 2

Figure 3 shows the 60-day time–height section of the equatorial zonal wind at 0° longitude reconstructed from the eastward-propagating zonal wavenumber 1 disturbances of all frequencies. The SKYHI results are shown in panel (a) and those from the linear model in panel (b). If one ignores for the moment the larger amplitude of fluctuations in the linear model, then there is an impressive similarity between the SKYHI and linear model simulations. In the middle atmosphere both models display the downward phase propagation and upward propagation of temporal wave packets expected for Kelvin waves excited in the troposphere. In both models the dominant vertical wavelengths in the stratosphere are about 12–15 km and the periods are near 12–14 days. These scales are consistent with Kelvin waves with zonal phase speeds of the order of 30–40 m s^{-1} and are similar to those of the "slow" Kelvin waves first observed by Wallace and Kousky (1968). In the mesosphere of both models, higher-frequency oscillations occur with vertical wavelength of about 25 km or more (particularly strong around day 32 and after day 62).

The altitude variation of the dominant frequency (and vertical wavelength) for fixed zonal wavenumber has also been seen in observations (Salby et al. 1984) and in previous numerical simulations (Hayashi et al. 1984; Garcia and Salby 1987). The high-frequency waves in the SKYHI mesosphere have properties sim-

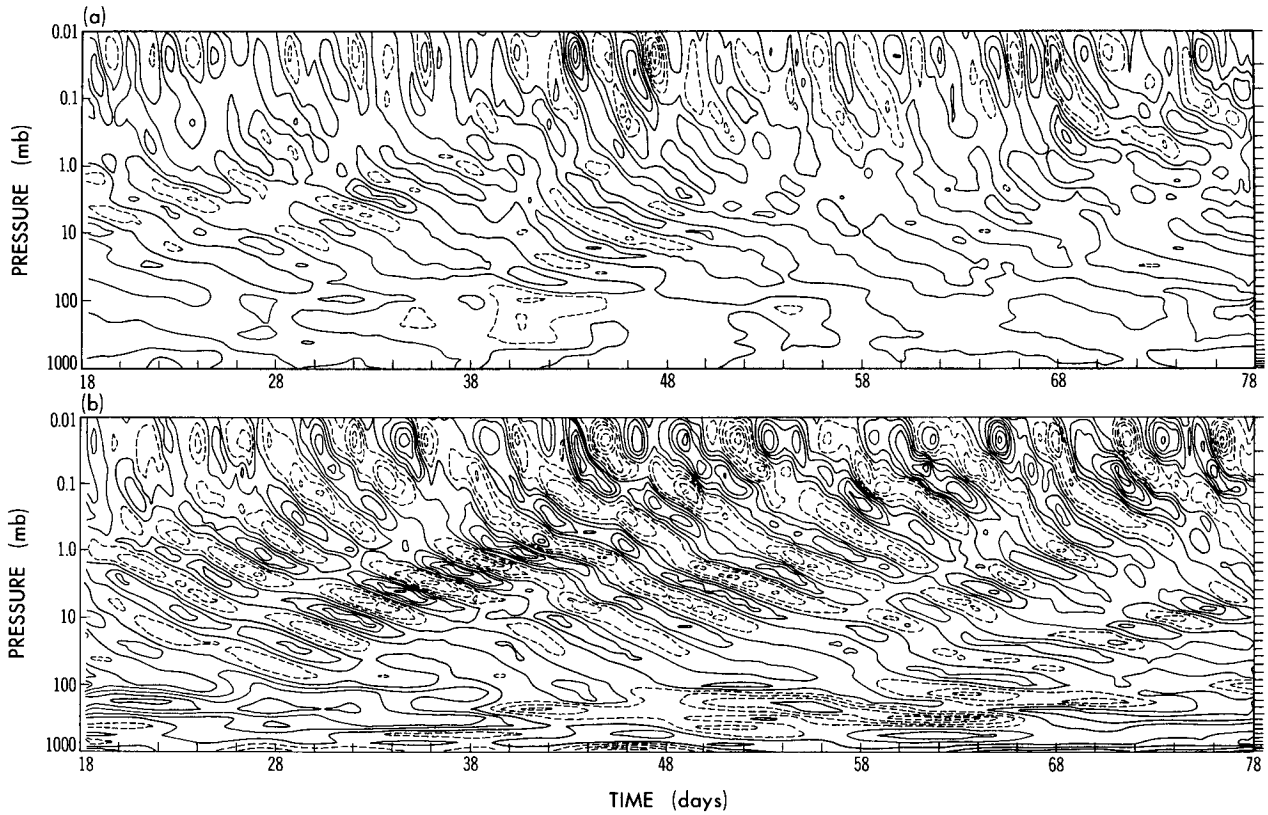

FIG. 4. As in Fig. 3 but for eastward-propagating wavenumber 2.

ilar to the "ultrafast" Kelvin waves seen in satellite data by Salby et al. (1984).

The agreement between the SKYHI and linear model results in Fig. 3 often extends beyond general appearance to a nearly exact correspondence of wave packets and of individual crest and trough positions. For example, in both simulations a wave packet can be clearly traced from the upper troposphere around day 36 to the stratopause at about day 68. In the center of the wave packets (i.e., where amplitudes are large) there is very close agreement in wave phase between the two models. Figure 3 clearly shows that the 18-day spinup time for the linear model is inadequate for wavenumber 1. The agreement between the two models in the upper stratosphere and mesosphere indeed improves during the last 30 days shown.

Figure 4 shows the corresponding equatorial zonal wind fluctuations for eastward-propagating wavenumber 2. Again the overall appearance of downward phase velocity and upward group propagation of well-defined pulses is consistent with earlier observations of wavenumber 2 in the equatorial middle atmosphere (e.g., Salby et al. 1984; Coy and Hitchman 1984). The dominant vertical wavelengths are similar to those for wavenumber 1 ($\sim$12 km in the stratosphere to more than 20 km in the mesosphere). The dominant periods in Fig. 4 are $\sim$5–6 days in the stratosphere (i.e., roughly a factor of 2 less than for wavenumber 1). There are several distinct wave packets that can be traced in both panels of Fig. 4, in particular those starting at about 100 mb near day 18, day 27, day 39, day 56, and day 64. The last two of these are rather weak and are more easily seen in the linear model results (but are also clearly present in the SKYHI simulation). The vertical group propagation appears to be somewhat faster in SKYHI than in the linear model, although Figs. 4a and 4b actually show very impressive agreement at least up to 0.1 mb when laid directly over one another. In contrast to wave 1, the 18-day spinup period appears to be adequate for wave 2 with its faster group velocity.

Figure 5 shows the latitude–time section of the 10-mb zonal wind associated with eastward-propagating wave 2. The results for both SKYHI and the linear model feature an equatorially trapped signal that agrees well with expectations for a Kelvin wave with phase speed $\sim$30–40 m s^{-1}. The agreement in phase between the two simulations near the equator is spectacular, particularly when the wave pulses are strong. At higher latitudes one sees longer period fluctuations, which presumably reflect the presence of quasi-stationary planetary waves. While both models have such mid-latitude variations, there is no agreement in the details

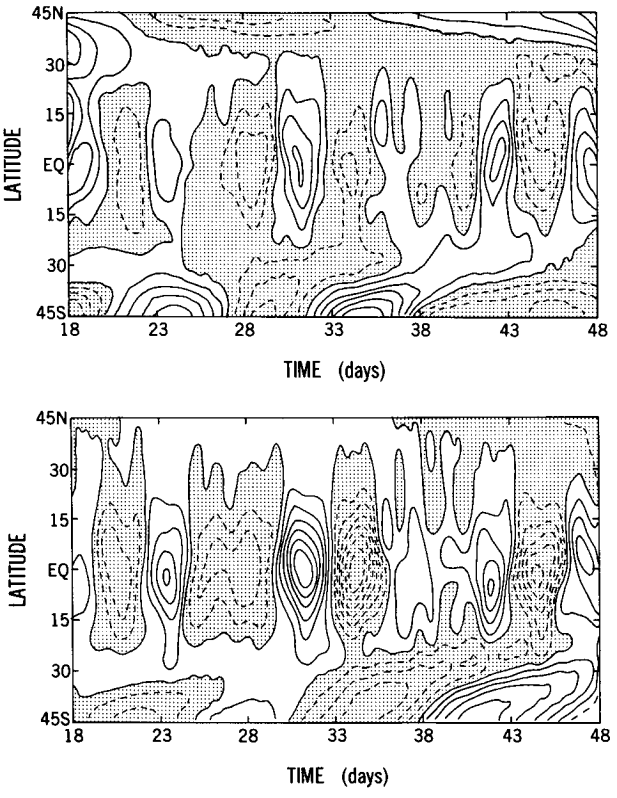

FIG. 5. Time–latitude sections of the zonal wind for eastward-propagating wavenumber 2 at 10 mb and 0° longitude over the M1 period; (top) SKYHI and (bottom) linear model. Contour interval: 1 m s^{-1}. Dashed contours indicate easterly winds. These figures have been slightly smoothed by taking a running mean over one day and applying a 1–2–1 averaging over the 3° latitude grid.

of the phase propagation. This is understandable since such waves are presumably strongly influenced by topography (which is not included in the linear model) as well as by diabatic forcing at latitudes poleward of 43.5° (also omitted in the linear model).

Similar conclusions can be drawn from a comparison of the latitude–time sections for wavenumber 1 (not shown).

The temperature variations associated with eastward-propagating wavenumbers 1 and 2 were examined and found to have very similar behavior to the zonal wind fluctuations. The very same wave pulses are clearly seen in the temperature field. The temperature variations are very nearly in quadrature with those of the zonal wind (not shown). The fluctuations in equatorial meridional wind associated with eastward-propagating waves 1 and 2 were also examined and found to be much weaker than the corresponding zonal wind fluctuations (consistent with the view that equatorial Kelvin waves dominate the eastward-propagating wave field).

For wave one (Fig. 3) the largest zonal wind amplitudes in SKYHI are ~5 m s^{-1}, which occur near 10 mb in the peak of the wave pulse around day 58. This is less than the 8 m s^{-1} value quoted as a typical amplitude of the Wallace–Kousky wave in the lower stratosphere during the easterly phase of the QBO (Wallace and Kousky 1968; Wallace 1973). For wave two, the peak amplitude near 10 mb is also ~5 m s^{-1}. Taking the waves 1 and 2 together, the *peak* amplitude becomes comparable to that estimated by Wallace and Kousky as the *typical* amplitude. On this basis it seems reasonable to conclude that on average the stratospheric Kelvin waves in SKYHI are somewhat weaker than observed.

The amplitude of each of the wave 1 and 2 Kelvin waves is clearly larger in the linear model than in the SKYHI simulation (see Figs. 3–5). The difference is evident at all levels, but above the tropopause the ratio of linear amplitudes to SKYHI amplitudes grows with height (particularly evident in Fig. 4 for wavenumber 2). By 10 mb the linear model waves are about twice as strong as those in SKYHI. The most obvious interpretation would be that the dissipation in SKYHI is stronger than that in the linear model. Explicit calculations with reduced K_H in the linear model showed that the horizontal diffusion does not play a significant role in damping the large-scale Kelvin waves (see M92). The radiative damping was designed to be similar in the two models (although there cannot be exact agreement given the simple Newtonian cooling scheme used in the linear model). A notable difference in the two models is the presence of the Richardson number–dependent vertical mixing and dry convective adjustment in SKYHI. When the linear solution for all waves is resynthesized there are frequent occurrences of locally unstable lapse rates (see M92). Thus, it seems probable that the nonlinear vertical mixing parameterizations act to constrain amplitudes of the vertically propagating waves in SKYHI. There are also differences between the amplitudes in the two simulations at the tropopause and in the troposphere itself (where high-frequency motions are much stronger in the linear model). These may reflect the absence of both vertical mixing and surface drag in the linear model.

b. Results for westward-propagating wavenumbers 1 and 2

Figure 6 shows time–height sections of the equatorial zonal wind fluctuations associated with westward-propagating zonal wavenumber 1 for both SKYHI and the linear model. Clearly there are significant differences between the westward planetary-scale waves in the SKYHI and linear models. A succession of disturbances with quasi-barotropic vertical structure is seen in the mesosphere of SKYHI. For instance, a pulse of waves with an 8–9-day period is apparent between days 24 and 42 in Fig. 6a. Another pulse extending into the upper stratosphere with a 16-day period occurs between days 54 and 70. Superimposed on these long-period

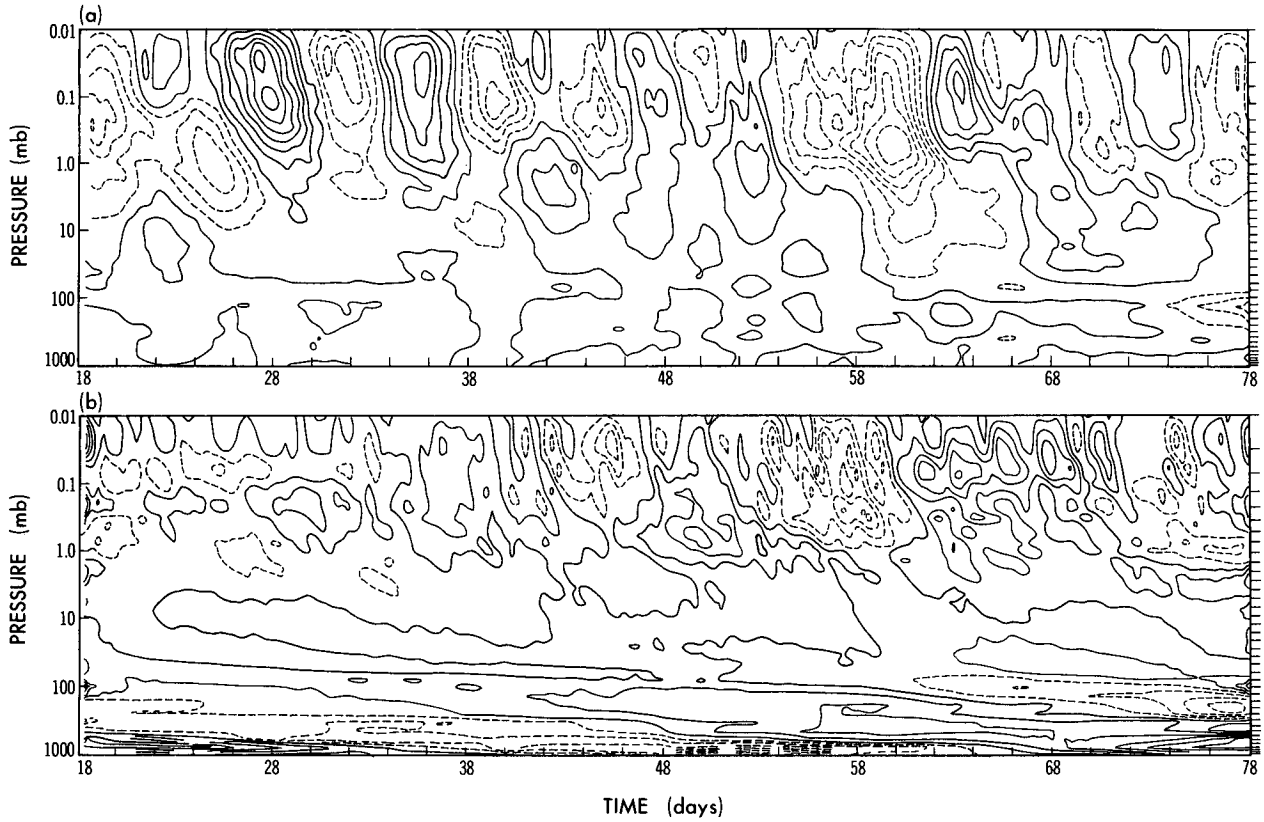

FIG. 6. As in Fig. 3 but for westward-propagating wavenumber 1.

pulses are other rather barotropic features of shorter period (for instance, around day 48). Corresponding disturbances are difficult to find in the linear solution (Fig. 6b). This difference between the SKYHI and linear model simulations is also apparent for wave 2 (not shown). In section 6 it will be demonstrated that the fluctuations in the SKYHI middle atmosphere reflect the presence of global Rossby normal modes. The corresponding modes are much weaker in the linear model simulation.

c. *Results for zonal wavenumbers 3 and 4*

The equatorial time–height sections corresponding to Figs. 3 and 4 were also computed for the eastward-propagating wavenumber 3 and 4 components. These figures (see M92) reveal the presence of vertically propagating Kelvin wave pulses quite similar to those seen for waves 1 and 2, but with higher frequencies and smaller amplitudes. The dominant periods in the stratosphere are about 4 days for wave 3 and 2–3 days for wave 4. These periods, and the dominant vertical wavelengths of about 15 km, are similar for SKYHI and the linear model. In both models, eastward-propagating waves 3 and 4 have higher frequencies and longer vertical wavelengths (~20–25 km) in the mesosphere. The peak zonal wind amplitudes of waves 3 and 4 in the stratosphere are a factor of 2–3 smaller than for wave 1 or 2. As for waves 1 and 2, the amplitudes of waves 3 and 4 in the linear model are a factor of ~1.5–2 larger than in SKYHI.

The equatorial zonal wind field associated with westward-propagating zonal waves 3 and 4 is much weaker than for the corresponding eastward waves. There is no evidence in waves 3 and 4 for the quasi-barotropic fluctuations so clearly seen in westward-propagating zonal wavenumbers 1 and 2 in the SKYHI simulation (e.g., Fig. 6). It is worth noting that the published observational studies have not found evidence for the zonal wavenumber 3 and 4 Rossby normal modes (with the exception of the identification of the observed "2 day" wave with the wavenumber 3 Rossby–gravity mode, e.g. Salby 1981b).

In observations, a prominent vertically propagating Rossby–gravity wave with dominant zonal wavenumber ~3–4 is evident in the meridional wind field in the equatorial stratosphere (Yanai and Maruyama 1966; Wallace 1973). A similar feature can be seen in the westward-propagating wavenumber 3 component in both the SKYHI and linear model simulations. The cleanest example of a Rossby–gravity wave pulse is illustrated in Fig. 7, which is a time–height section of

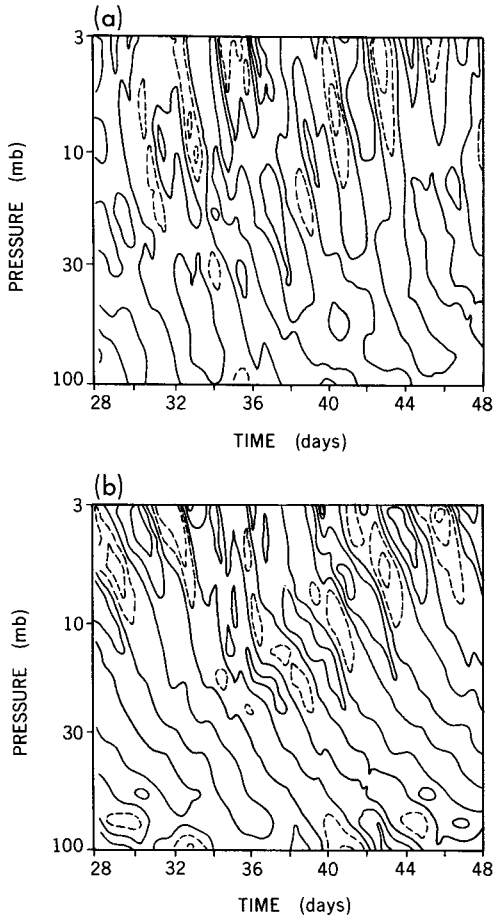

FIG. 7. Time–height section of the equatorial meridional wind for westward-propagating wavenumber 3 at 0° longitude. Results shown for 20 days and only from 100–3 mb. (a) SKYHI and (b) linear model. Contour interval 1 m s^{-1}.

the westward-propagating wave 3 component of the equatorial meridional wind. A wave pulse propagates from 100 mb at day 28 to 3 mb at day 44. The dominant wave period is ~4 days and the vertical wavelength is ~5–6 km; both these features are similar to the observed Yanai–Maruyama wave. The amplitudes of the meridional velocity fluctuations associated with the observed Yanai–Maruyama wave in the lower stratosphere have been estimated to be ~2–3 m s^{-1} (Wallace 1973). It appears that the corresponding wave in the both SKYHI and the linear model is much weaker. The peak amplitude of the wave pulse in Fig. 7 significantly exceeds 1 m-s^{-1} only above 10 mb, and this is the strongest event seen in the entire 60-day period. The comparison with observations is not straightforward, since Wallace quotes values appropriate for weak mean westerlies, while the present models have mean easterlies in the tropical lower stratosphere, but it is hard to avoid the conclusion that the Yanai–Maruyama wave in SKYHI is unrealistically weak. The meridional wind field is shown only up to 3 mb in Fig. 7. Above this level the meridional wind fluctuations are dominated by rather irregular disturbances with periods shorter than 3 days and with much longer vertical wavelengths (~25 km or more).

For zonal wavenumber 4 there is some indication of an even weaker westward-propagating Rossby–gravity wave with period near 3 days and vertical wavelength ~6 km (not shown). This is apparent only below about 50 mb.

d. The thermal forcing

Figures 8 and 9 show time–height sections of the meridionally averaged (from 10.5°S to 10.5°N) thermal forcing for the eastward- and westward-propagating wavenumber 1, respectively. Only the bottom 16 levels, ranging from 100 mb to 1000 mb, are shown. The heating rates have been slightly smoothed by means of a daily running mean. The thermal forcing is very coherent vertically, and (when expressed as the heating per unit mass) generally peaks around 500 mb. A very rough estimate of the dominant vertical scale of the thermal forcing might be 8–10 km.

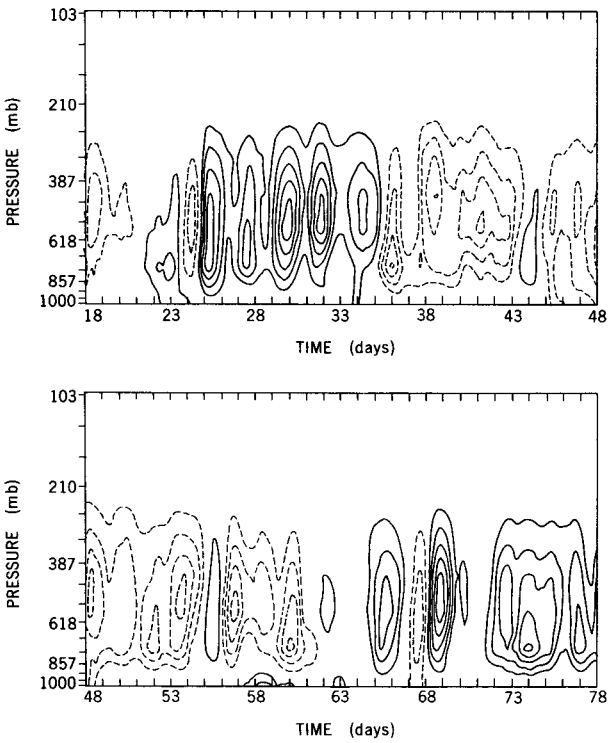

FIG. 8. Time–height sections of thermal forcing for eastward-propagating wavenumber 1, at 0° longitude and meridionally averaged over 10.5°S–10.5°N. The (top) M1 period and the (bottom) M2 periods are shown. Contour interval: 0.1 K day^{-1}. Dashed contours indicate negative values. The zero contour is not plotted. The data have been slightly smoothed by taking a one-day running mean. The tick marks on the vertical axis indicate the positions of model levels. The space–time Fourier decomposition was done separately for the M1 and M2 periods; thus, there are discontinuities at the boundary between the panels.

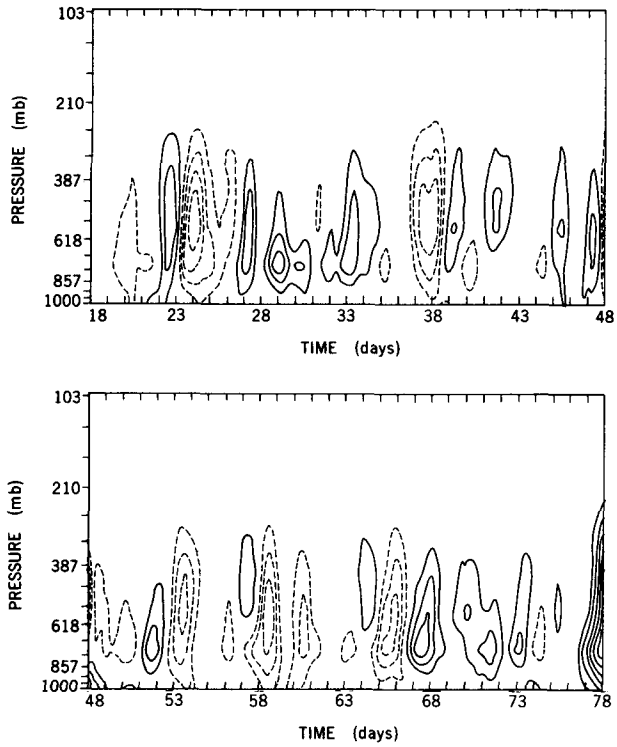

FIG. 9. As in Fig. 8 but for westward-propagating wavenumber 1.

The most prominent variation of the eastward component of the forcing is a long (~30–40 day) period modulation. This feature is notably absent in the westward component, which has a dominant period of oscillation of the order of a few days. It is natural to associate the long period variation in Fig. 8 with the Madden–Julian oscillation (Madden and Julian 1972), which appears as a large-scale eastward-propagating precipitation maximum in the tropics.

In Fig. 8 there is no prominent signal corresponding to the 12–14-day period of the wavenumber 1 stratospheric Kelvin wave signal. The stratospheric response in Fig. 3b is strikingly more periodic than the thermal forcing.

The time–latitude sections of the vertically integrated thermal forcing for wavenumber 1 were also computed (not shown). The forcing presented in this way looks rather noisy, with significant meridional coherence generally extending only over two or three grid points (6–9 degrees of latitude). Centers of strong forcing mostly cluster around the equator, but also appear at higher latitudes. There is a modest, but clearly discernible, shift of the forcing into the Northern Hemisphere in the M2 period.

e. Discussion

The large-scale eddy circulation in the SKYHI equatorial stratosphere is dominated by eastward-propagating Kelvin waves. For each individual zonal wavenumber, the equatorial zonal wind and temperature fields display roughly periodic oscillations with an amplitude that is modulated so that most activity is concentrated into well-defined upward-propagating pulses. The period of the dominant stratospheric oscillation decreases with wavenumber, so that the horizontal phase speed is roughly 30–40 m s^{-1} for each of zonal wavenumbers 1–4. The same vertical wavelength of ~12–15 km is characteristic of each individual wavenumber. The wavenumber 1 and 2 Kelvin waves in SKYHI have properties very similar to those of the observed Wallace–Kousky wave, although observations suggest that the dominant phase speed is somewhat smaller (~25 m s^{-1}; e.g., Wallace 1973) than found in the model.

The stratospheric Kelvin wave field in SKYHI is well reproduced by the linear model. Thus, it appears that heating by the convective parameterization is the principal source of excitation for these waves in SKYHI. The impressive periodicity of the stratospheric waves is consistent with Holton's (1973) finding that the vertical wavelength and horizontal phase speed of Kelvin waves forced by a broad spectrum of tropospheric heating are largely determined by the vertical scale of the forcing. There is no indication that wave–CISK plays any role in forcing the stratospheric Kelvin waves. On the other hand—given the prominent long period modulation of the eastward-propagating thermal forcing—it is tempting to speculate that wave–CISK may be crucial in forcing the Madden–Julian oscillation in SKYHI.

Higher-frequency Kelvin waves appear to dominate the eastward-propagating component of the wave field in the equatorial mesosphere of SKYHI. A shift to higher frequencies with height is to be expected, since (for fixed zonal wavenumber) the lower-frequency waves have slower vertical group velocity and are selectively filtered by any dissipation. By the mesopause the dominant phase speeds may exceed 100 m s^{-1}. These very fast Kelvin waves are also seen in the linear simulation, suggesting that they are excited by tropospheric convective heating.

The good agreement between SKYHI and linear simulations for the eastward waves 1 and 2 contrasts strongly with the situation for the global-scale westward waves. For westward-propagating waves 1 and 2, the upper stratosphere and mesosphere is dominated by quasi-barotropic fluctuations that appear to be only weakly excited in the linear simulation.

For waves 3 and 4, there is some suggestion in both models of a weak westward-propagating signal corresponding to the observed Yanai–Maruyama wave. When this wave is relatively strong, the amplitude in the linear model is comparable to or larger than that in SKYHI. Thus, convective heating appears able to account for the excitation of the Yanai–Maruyama wave in SKYHI.

5. Smaller-scale waves

Figure 10 shows the space–time power spectrum for the equatorial zonal wind at 1.08 mb for both the SKYHI and linear simulations. Power is concentrated in two regions, one with eastward phase speeds of ~30–50 m s^{-1} and another with westward phase speeds of about the same magnitude (consistent with earlier studies, e.g., Hamilton and Mahlman 1988). For westward-propagating wavenumbers 1–3 in SKYHI, there is also a center at low frequencies (around 0.1 day^{-1}), which is not apparent in the linear model. This presumably reflects the presence of prominent Rossby normal modes in the SKYHI simulation (see section 6 below).

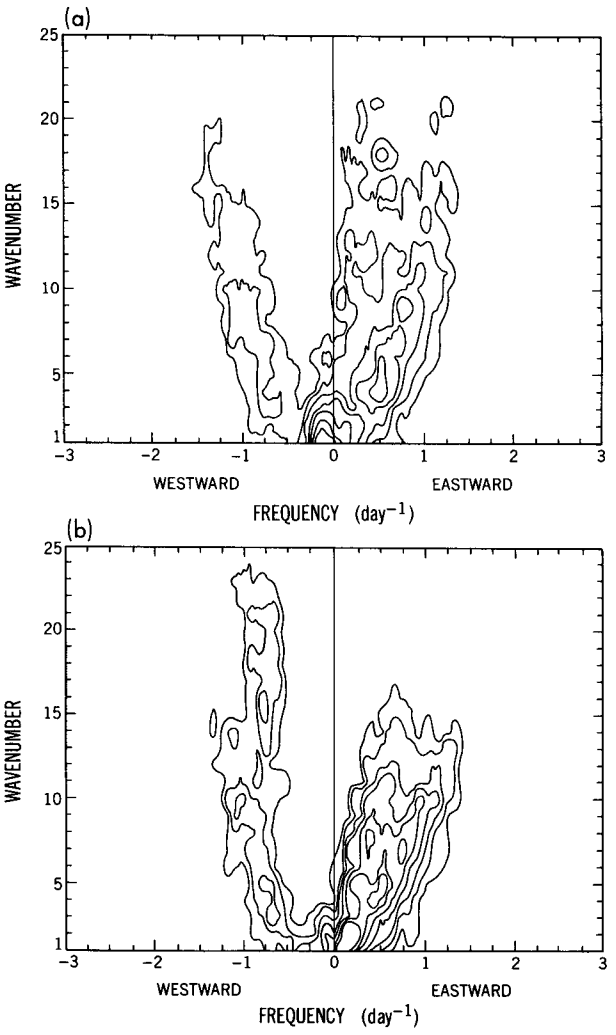

FIG. 10. Space–time power spectrum of the equatorial zonal wind at 1.08 mb for (a) SKYHI and (b) linear model. The contour value doubles at each interval, starting from 0.5 m^2 s^{-2} day. The zero frequency is not included in this analysis. The fields have been smoothed by means of a running mean over five adjacent Fourier frequencies (i.e., over a bandwidth of 0.167 day^{-1}).

While the power in both models drops off with increasing wavenumber, there is a substantial fraction of the variance at less than planetary scales. The spectrum becomes less red at higher altitudes. The spectrum of vertical momentum transport emphasizes the higher wavenumbers even more, and the fluxes from the small-scale waves can significantly affect the general circulation of both the tropics and extratropics (e.g., Miyahara et al. 1986; Hamilton and Mahlman 1988). In this section the motions with zonal wavenumbers greater than 4 will be compared in the linear and nonlinear models. In what follows, the sum of all wavenumbers > 4 will be examined and will be loosely referred to as the "inertia–gravity" (IG) wave field.

a. Comparison of results in the control runs

Figure 11 shows a time–height section of the equatorial zonal wind at 0° longitude when all eastward-propagating waves with zonal wavenumber > 4 are resynthesized. The overall pattern of downward phase propagation and upward group propagation is apparent in both models, as is a clear tendency for the dominant frequencies and vertical wavelengths to increase with height. In the mesosphere the dominant period appears to be somewhat over 1 day. In SKYHI, the amplitude of the IG wave field is comparable to that of the planetary-scale Kelvin waves in the stratosphere and is actually larger in the mesosphere (note that the contour interval in Fig. 11 is twice that in Figs. 3 and 4). While the linear and full GCM simulations have similar wave periods and wavelengths, it is not possible to find much agreement in the positions of individual crests and troughs. This lack of detailed agreement is not surprising for small-scale waves, since in the linear model the only advective effects on wave propagation are those associated with the zonal mean. It does seem possible, however, to identify some of the same wave pulses in the two simulations—notably one traveling from about 10 mb at day 28 to 0.01 mb at day 32, and one from near 10 mb at day 38 to 0.01 mb at day 44.

Figure 12 shows the same analysis but for westward-propagating IG waves. The overall appearance of this time–height section is similar to that seen for the eastward waves, but the westward wave amplitudes are somewhat smaller and the dominant frequency is somewhat higher. The differences may reflect the effects of the mean easterlies in the tropical stratosphere (see Fig. 1a) in filtering out the slower westward-propagating components of the spectrum. In this case the two most obvious wave pulses in the SKYHI simulation show up clearly in the linear solution as well (days 26–30 and days 40–43).

Equatorial time–height sections corresponding to Figs. 11 and 12 were produced for several other longitudes. While there is little detailed correlation between time series at locations widely separated in lon-

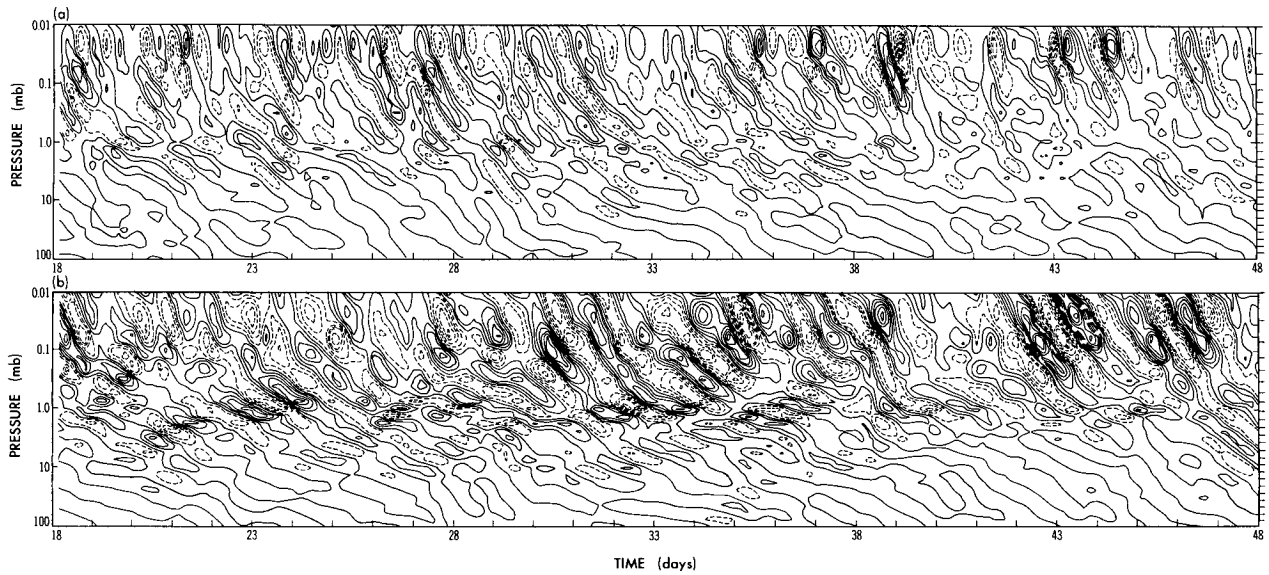

FIG. 11. Time–height section of the equatorial zonal wind for the sum of all eastward-propagating disturbances with zonal wavenumber > 4 at 0° longitude over the M1 period. (a) SKYHI and (b) linear model. Contour interval: 4 m s^{-1}. Dashed contours indicate easterly winds.

gitude, the general agreement between the SKYHI and linear solutions is found at each longitude.

Figure 13 shows the vertical component of the Eliassen–Palm (EP) flux associated with the eastward-propagating IG waves in both models during the M1 period. The isobaric coordinate form of the EP flux is used along with the sign convention of Andrews et al. (1983). Thus, positive values represent upward eddy fluxes of westerly momentum. Note that the negative values in Fig. 13 occur in regions of strong mean westerlies, where much of the eastward-propagating component of the spectrum might be traveling westward relative to the mean flow. Near the equator in Fig. 13, both models have comparable fluxes emerging into the stratosphere. The equatorial values of the flux drop off with height and the wave fluxes appear to spread out to higher latitudes. Equatorward of about 20° the fluxes in the SKYHI and linear models agree quite well, but by 25°–30° latitude the flux in the linear simulation is significantly less than in the full GCM. It seems log-

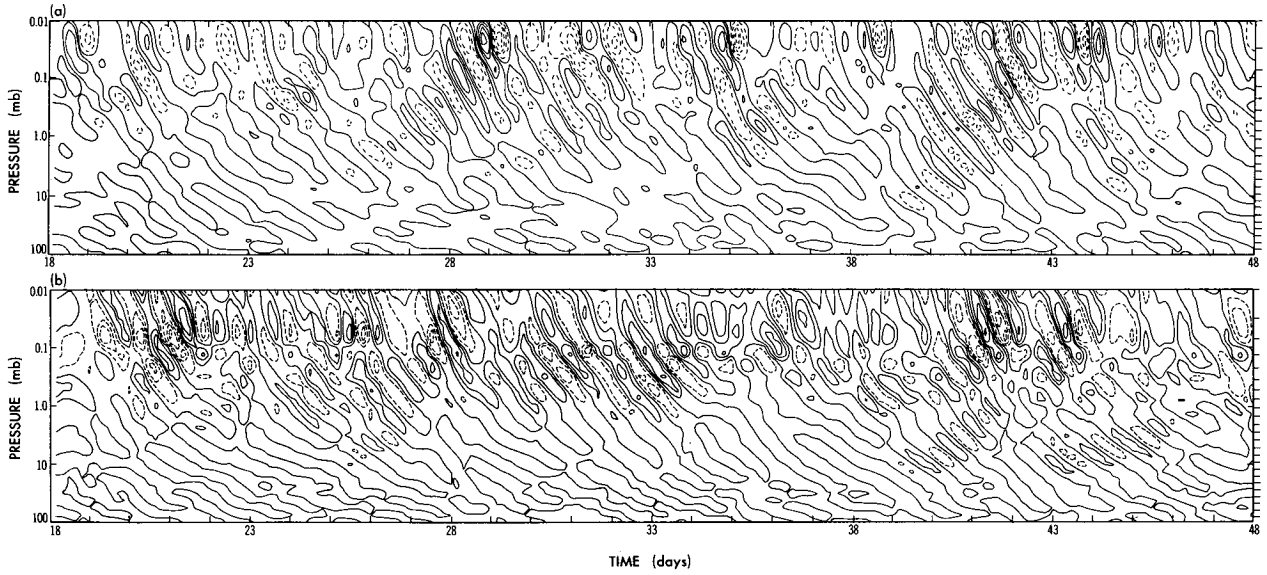

FIG. 12. As in Fig. 11 but for westward-propagating wavenumbers > 4.

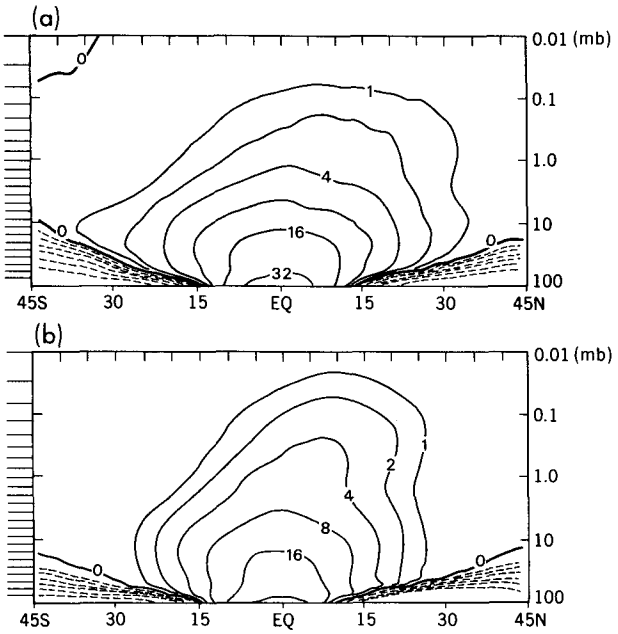

FIG. 13. Meridional cross sections of the vertical EP flux for eastward-propagating wavenumbers > 4, averaged over the M1 period. (a) SKYHI and (b) linear model. The contour labels represent multiples of 0.25×10^{-5} m mb s^{-2}. Dashed contours indicate negative fluxes. The tick marks on the vertical axis indicate the positions of model levels.

ical to conclude that other sources contribute significantly to the IG wave field in the SKYHI subtropics. In both the SKYHI and linear results, the fluxes are larger in the Northern Hemisphere than in the Southern Hemisphere and this difference increases with height. This asymmetry is presumably caused by the filtering effects of the mean westerlies in the Southern Hemisphere middle atmosphere (Fig. 1).

The results for the vertical EP fluxes associated with the westward-propagating IG waves in the M1 period are shown in Fig. 14. Near the equator the fluxes in the two models are nearly equal, but the magnitude of the linear model flux is noticeably less than that in SKYHI poleward of about 15°. In both cases the fluxes decrease much less rapidly in the Southern Hemisphere (where there are strong mean westerlies).

The vertical component of the EP flux for the westward-propagating IG waves during the M2 period in the two models was also compared. Again there was found to be good agreement between the two simulations at low latitudes, but the SKYHI fluxes become significantly stronger than the linear fluxes in the subtropical stratosphere. The interhemispheric asymmetry of propagation is enhanced over that seen in the M1 period, presumably reflecting the intensification of the Southern Hemisphere westerly jet and the Northern Hemisphere easterly jet (see Fig. 1).

The results in Figs. 11–14 suggest that the tropospheric thermal forcing considered here can account for essentially all the gravity wave activity found in SKYHI near the equator and may also be responsible for a substantial part of the IG wave field even in the extratropics. Figure 15 is the time–height section of the IG zonal wind field for eastward-propagating waves for a location at 30°N. The SKYHI results in Fig. 15a look rather similar to those at the equator, in that downward phase propagation is evident almost all the time. The dominant periods here are shorter than at the equator; this is expected since vertically propagating IG waves must have intrinsic angular frequency greater than the local Coriolis parameter. The linear model results in 15b look very different in the stratosphere, with very weak amplitudes and almost random phase propagation. Above about 1 mb strong pulses appear in both models. Periods of strong activity in the SKYHI mesosphere around days 18–22, 26–28, 29–32, 38–40, and 42–44 all have corresponding pulses in the linear model simulation. A similar pattern is seen in the corresponding plots for the westward-propagating IG waves at 30°S (not shown). In this case days 26–31, days 40–44, and days 46–48 appear as periods of intense mesospheric activity in both models.

An obvious interpretation of the linear model results in Fig. 15 would be that mesospheric wave pulses arrive from lower latitudes, and that there is little direct propagation upward from subtropical tropospheric sources (accounting for the very weak amplitudes seen in the stratosphere in Fig. 15b). The SKYHI results show many of the same mesospheric wave packets (presumably also excited by low-latitude tropospheric convection) as well as additional wave activity in both the

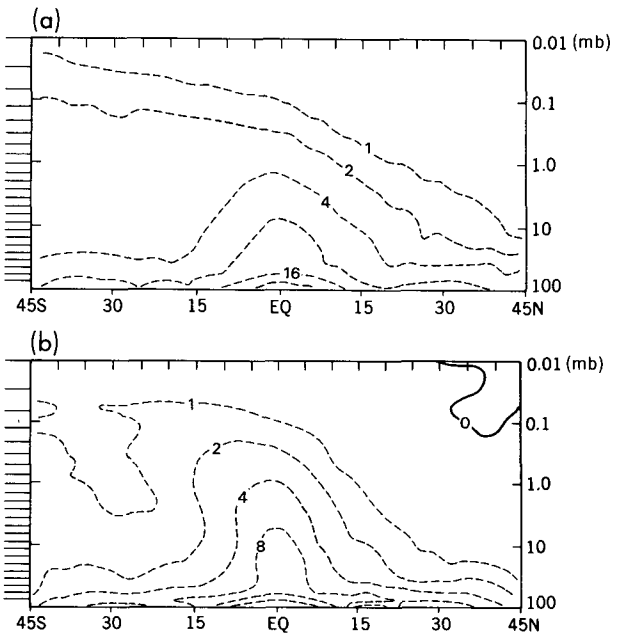

FIG. 14. As in Fig. 13 but for westward-propagating disturbances with zonal wavenumber > 4. Results for the M1 period.

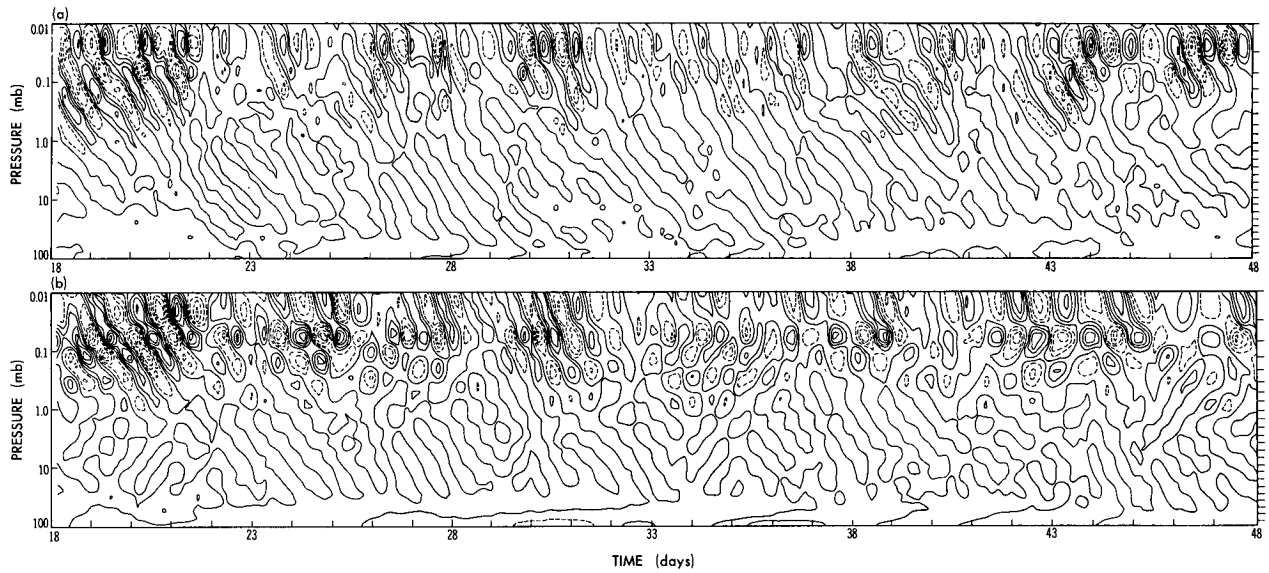

FIG. 15. Time–height sections of the zonal wind for eastward-propagating wavenumbers > 4 at 30°N and 0° longitude over the M1 period. (a) SKYHI and (b) linear model. Contour interval: 4 m s^{-1}. Dashed contours indicate easterly winds.

stratosphere and mesosphere generated by mechanisms not included in the linear model.

Manzini (1992) presents height–time sections similar to those in Figs. 15 for 43.5°N and 43.5°S. At these higher latitudes the dominant wave periods are even shorter, but the overall pattern of large mesospheric pulses is similar to that seen at 30° latitude.

Manzini also computed the EP flux vectors separately for the westward- and eastward-propagating IG waves in both the linear and full SKYHI models. The correspondence between the two models at low latitudes is quite striking. In each case the direction of the EP fluxes indicate the presence of a dominant low-latitude tropospheric source with flux spreading upward and poleward in the stratosphere. In the middle atmosphere away from the equator, the fluxes show strong hemispheric asymmetry, with the westward waves propagating effectively only in the Southern Hemisphere (where there are mean westerlies) and the eastward waves propagating only into the Northern Hemisphere. In the case of the westward-propagating IG waves, the total EP flux remains poleward (using the sign convention of Andrews et al. 1987; this corresponds to a poleward flux of wave activity) in the linear model to at least 43.5°N. By contrast, in SKYHI the poleward EP flux component diminishes with latitude, so that by 43.5°N there is perhaps a slight equatorward component of the EP flux. This result highlights the likely importance of higher-latitude sources for the gravity waves in the extratopics.

b. *Experiments with low-latitude forcing only*

The pattern of the EP fluxes shown in the linear model results in Figs. 13 and 14 suggests that the convective excitation is strongly concentrated near the equator and that the waves forced in the equatorial troposphere spread out over a considerable range of latitudes in the middle atmosphere. To investigate this further, the linear model simulation for the first 48 days was performed with the thermal forcing set to zero poleward of 4.5° latitude and then repeated with the forcing set to zero poleward of 10.5°. The results for the vertical EP flux associated with westward-propagating IG waves in these two experiments are shown in Figs. 16a and 16b, respectively. The waves forced at these low latitudes obviously do spread out over a wide meridional range in the stratosphere and mesosphere. It is striking how well these figures agree with those from the full linear simulation (Fig. 14), at least to about 15° latitude. Similar results were found for the eastward propagating IG waves (not shown).

c. *Thermal forcing*

Figure 17 is the time–height section of the thermal forcing for the wavenumber > 4 waves reconstructed at 0° longitude for the M1 period. As in Figs. 8 and 9, the heating rates have been averaged over 10.5°S to 10.5°N. In this case the results for westward-propagating waves are in panel (a) and for eastward-propagating waves in panel (b). The thermal forcing for these smaller scales has the strong vertical coherence that characterized the wavenumber 1 forcing examined earlier (Figs. 8 and 9). The heating rates in Fig. 17 appear to peak slightly lower than those in Figs. 8 and 9. The heating rate time series for both westward- and eastward-propagating waves in Fig. 17 feature prominent pulses of activity (days 28–34 and 43–46 in Fig. 17a, and days 18–23 in Fig. 17b), presumably asso-

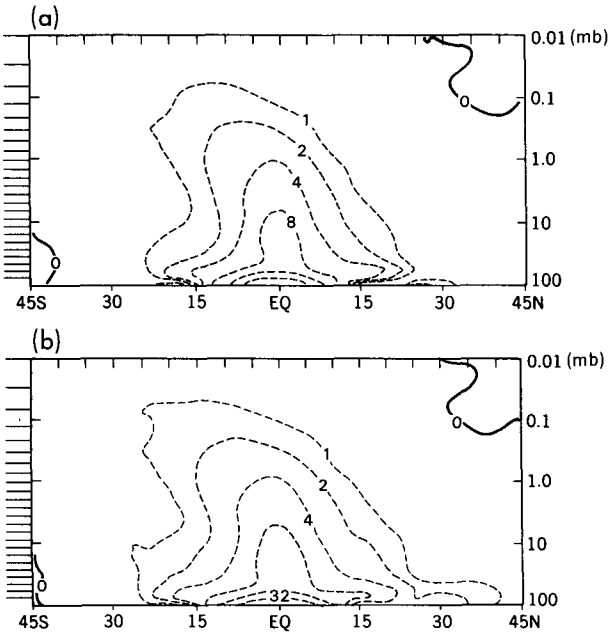

FIG. 16. As in Fig. 14 in the experiment with thermal forcing confined between (a) 4.5°S and 4.5°N, and (b) 10.5°S and 10.5°N.

ciated with the passage of synoptic systems. It is noteworthy that the difference in the behavior of the westward- and eastward-propagating thermal forcing components is much less pronounced in the wavenumber > 4 results than it is for the wave 1 results shown earlier (Figs. 8 and 9).

d. Discussion

The present results have shown that the convective heating is a very strong excitation for resolved IG waves in the SKYHI model. This forcing is typically very coherent over the depth of the troposphere. Thus, the tendency for the horizontal phase velocities to cluster around a 30–50 m s^{-1} range may be a result of the same selection mechanism operating in the case of the global-scale Kelvin waves (Holton 1973). The IG wave amplitudes in the equatorial lower stratosphere were similar in the linear and full SKYHI models. The near agreement for the IG waves contrasts with the earlier finding that the Kelvin waves in the linear model are actually stronger than those in SKYHI, even at the tropopause (section 4 above). The smaller-scale IG waves have faster vertical group velocities than the large-scale Kelvin waves, and thus should be less affected by dissipation. Hence, the fact that there is no vertical diffusion in the linear model may have little effect on the ratio of IG wave amplitudes in the linear model and SKYHI simulations (but have a large effect on the amplitude ratio for the global-scale Kelvin waves).

The linear model produces large IG wave fluxes in the extratropical mesosphere as well, suggesting that convective heating may be an important excitation for the waves observed in the midlatitude middle atmosphere.

Finally, it must be noted that the present calculations address only the part of the gravity wave spectrum explicitly resolved in the GCM. The real atmosphere has significant variance at higher frequencies and smaller horizontal scales than can be represented in a GCM (and these high-frequency waves may actually be associated with a large fraction of the vertical eddy momentum fluxes). The present study cannot assess the importance of the convective excitation for these high-frequency waves.

6. Rossby normal modes

As noted earlier, the westward-propagating wavenumber 1 and 2 fields in the SKYHI simulation are dominated in the mesosphere by fairly long period, nearly barotropic oscillations (e.g., Fig. 6). In this section it will be shown that these oscillations are identifiable with the Rossby normal modes that have been

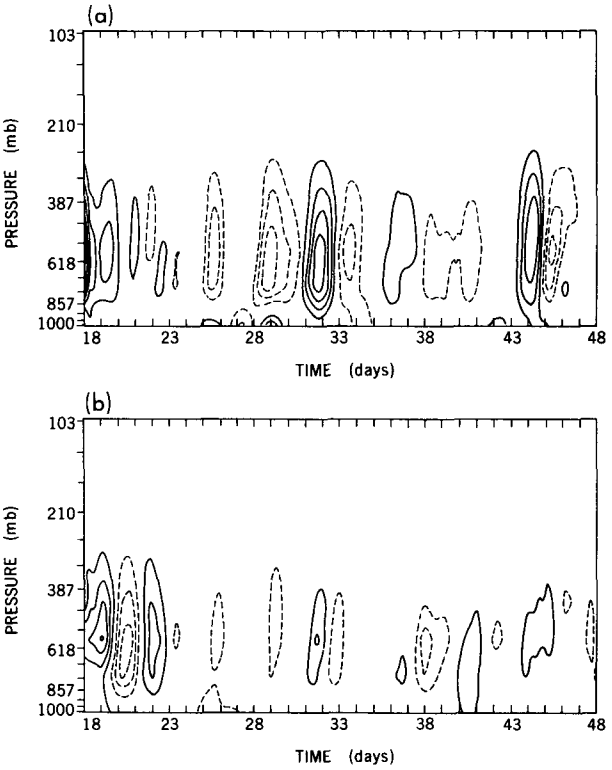

FIG. 17. Time–height sections of the thermal forcing for (a) westward-propagating wavenumbers > 4 and for (b) eastward-propagating wavenumbers > 4, at 0° longitude and meridionally averaged over 10.5°S–10.5°N. The M1 period is shown. Contour interval: 0.5 K day^{-1}. Dashed contours indicate negative values. The zero contour is not plotted.

detected in observations, such as the "16-day wave" and the "5-day wave" (see Salby 1984 for a review). Although this analysis is unfortunately restricted to the region equatorward of 45°, some unambiguous conclusions will be obtained. In particular, it will be demonstrated that the spectrum of normal-mode Rossby waves in the SKYHI model has some impressively realistic features. A comparison of the SKYHI simulation with that from the linear model will also be presented, allowing a direct determination of the significance of thermal forcing for normal modes in the full general circulation model.

Following the usual convention, the Rossby normal modes will be denoted by the two numbers: (s, n), where s is the zonal wavenumber and n is the meridional mode number (i.e., there are $n - 1$ zero crossings in the height field from pole to pole in the idealized no-mean flow solution). The meridional structures of the zonal wind and geopotential for the gravest few modes of a motionless atmosphere are given in Longuet-Higgins (1968), while the corresponding solutions in the presence of realistic mean flows are discussed in Salby (1981a). The range of periods associated with the Rossby normal modes observed in the upper stratosphere (Hirota and Hirooka 1984; Hirooka and Hirota 1985) is compared with those predicted by Salby (1981a) in Table 1.

a. Analysis for zonal wavenumbers 1 and 2

Figure 18 shows the time–latitude section of the westward-propagating zonal wavenumber 1 component of the 0.2-mb zonal wind when filtered to retain periods longer than 7.5 days. Results for both SKYHI and the linear model are presented. The SKYHI field (top panel) reveals somewhat irregular fluctuations with considerable meridional coherence. Overall, the results appear to be consistent with the presence of some mixture of low-order modes [particularly the antisymmetric (1,2) mode and the symmetric (1,3) mode]. The corresponding linear model field (lower panel) is quite different. The wind fluctuations are much weaker than in the SKYHI model and have no consistent agreement in phase (a striking contrast with the result for eastward waves in Fig. 5). The linear model disturbances in Fig. 18 are particularly weak in the first half of the record, possibly suggesting that a long spinup time is needed for the linear model. Even at the end of the 78-day integration, however, the agreement between the linear and SKYHI models is quite poor. This point is reinforced by examination of comparable time–latitude sections of the westward-propagating zonal wavenumber 2 (not shown). In this case as well, the SKYHI wind fluctuations are found to be much stronger than those in the linear model throughout almost the entire integration.

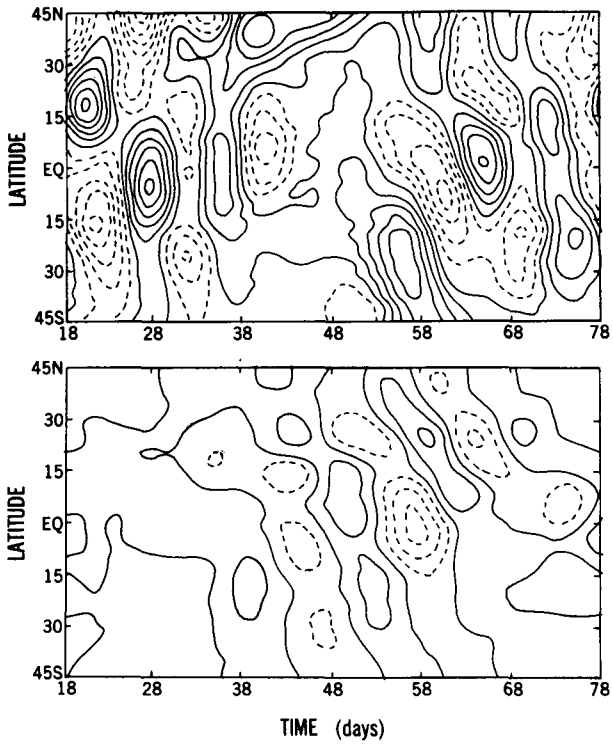

FIG. 18. Time–latitude section of the 0.2-mb zonal wind at 0° longitude for westward-propagating wavenumber 1 filtered to retain only periods longer than 7.5 days. Results for the M1 and M2 periods for SKYHI (top) and the linear model (bottom). The contour interval is 2 m s^{-1} and dashed contours denote easterly wind.

TABLE 1. Theoretically predicted periods of the gravest wavenumber 1 and 2 Rossby normal modes in the atmosphere from Salby (1981a). Also shown are the approximate observed period range from Hirota and Hirooka (1984) and Hirooka and Hirota (1985). The final column gives the names that have been used in the literature for the modes.

	Period range		
Mode	Theoretical (days)	Observed (days)	Name
(1,1)	4.4–5.7	5.0–6.0	5-day wave
(1,2)	8.3–10.6	7.5–12.0	10-day wave
(1,3)	11.1–20.0	12.0–24.0	16-day wave
(2,1)	3.8–4.8	4.0–5.0	4-day wave
(2,2)	6.6–7.7		
(2,3)	11.1–20.0		

In order to isolate individual modes in the SKYHI data, the wind and geopotential height variations for westward-propagating wavenumbers 1 and 2 were resynthesized for period ranges similar to those in Table 1. As an example, Fig. 19 shows westward-propagating wavenumber 1 zonal winds resynthesized over periods ranging from 15.6 to 26 days. This period range is a compromise between the few low frequencies resolved in a 78-day record and the band of periods suggested by earlier studies of the "16-day wave" (see Table 1).

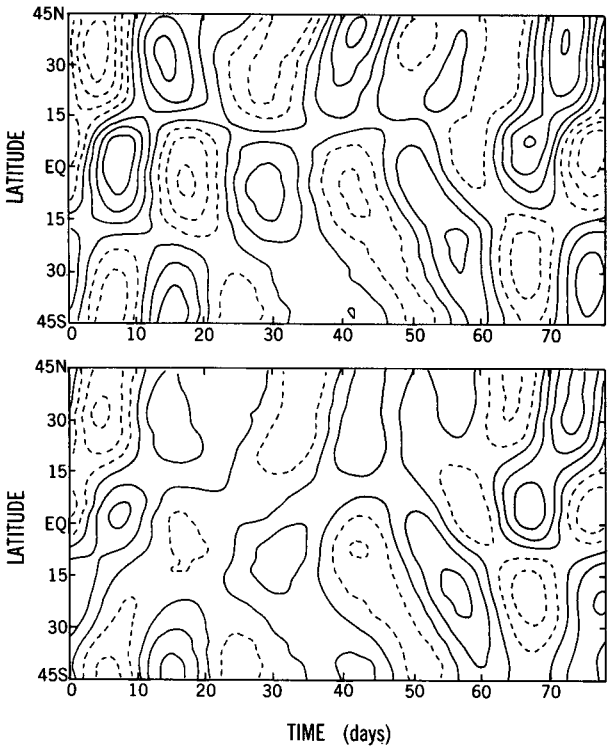

FIG. 19. Time–latitude section of the zonal wind at 0° longitude for westward-propagating wavenumber 1 filtered to retain only periods between 15.6 and 26 days. Results are for all 78 days of the SKYHI integration at 0.2 mb (top) and 1 mb (bottom). The contour interval is 2 m s^{-1} and dashed contours denote easterly wind.

The results for the entire 78-day SKYHI integration are presented for both the 0.2-mb and 1-mb levels. A zonal wind pattern resembling the idealized (1,3) mode is easily identified for the first 30 days. Local amplitude maxima occur at the equator and poleward of 30° in both hemispheres. These maxima are separated by nodal surfaces at about 15°N and 15°S. A clear signal of the (1,3) mode is not so apparent between days 30 and 60, but becomes well established once more after day 60. There is a near-exact coincidence of phase between the wind fluctuations at 0.2 and 1 mb at all latitudes, particularly when the (1,3) mode is strong. When the geopotential fluctuations in the SKYHI model were filtered in the same manner (not shown), the expected structure for the (1,3) mode was clearly revealed. The amplitude of the 1-mb geopotential height fluctuation in the filtered field at 43.5°N and 43.5°S is roughly 100 m, in agreement with the observations of the (1,3) mode by Hirooka and Hirota (1985).

Figure 20 shows the westward-propagating wavenumber 1 zonal wind field filtered to retain only periods between 4.6 and 6.7 days. Results are shown at 0.2 mb for both SKYHI (top) and the linear model (bottom). The SKYHI results show a very clean signal of the (1,1) mode, with maximum near the equator, a hint of a nodal point near 40° in each hemisphere, and strong meridional coherence. The corresponding geopotential fields for SKYHI (not shown) also agree with theoretical expectations for the (1,1) mode. The 0.1-mb geopotential height amplitude for the (1,1) mode near 45° latitude in the SKYHI simulation is of the order of 50 m, in rough agreement with the findings of Hirota and Hirooka (1984). The linear model simulation also has a clear signal of a (1,1) normal mode, but the amplitude is much smaller than that seen in SKYHI (note the contour interval in the bottom panel of Fig. 20 is one-quarter that of the top panel). There is also very little agreement between the phase of the (1,1) mode in the two simulations.

Mazini (1992) gives further details of the attempt to isolate individual modes. The "4-day wave" or (2,1) mode can be very clearly detected in the SKYHI simulation, but is virtually absent from the linear model results. The antisymmetric modes (1,2) and (2,2) are rather more difficult to see in pure form. Even in observations it is apparently difficult to separate the (2,2) and (2,3) modes (Hirooka and Hirota 1985).

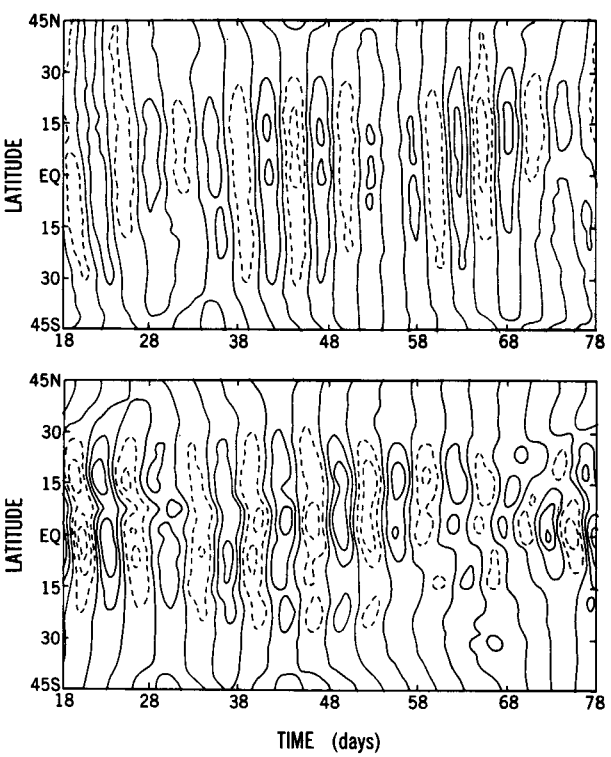

FIG. 20. Time–latitude section of the zonal wind at 0° longitude for westward-propagating wavenumber 1 filtered to retain only periods between 4.6 and 6.7 days. The top panel is for SKYHI and the contour interval is 2 m s^{-1}. The bottom panel is for the linear model and the contour interval is 0.5 m s^{-1}.

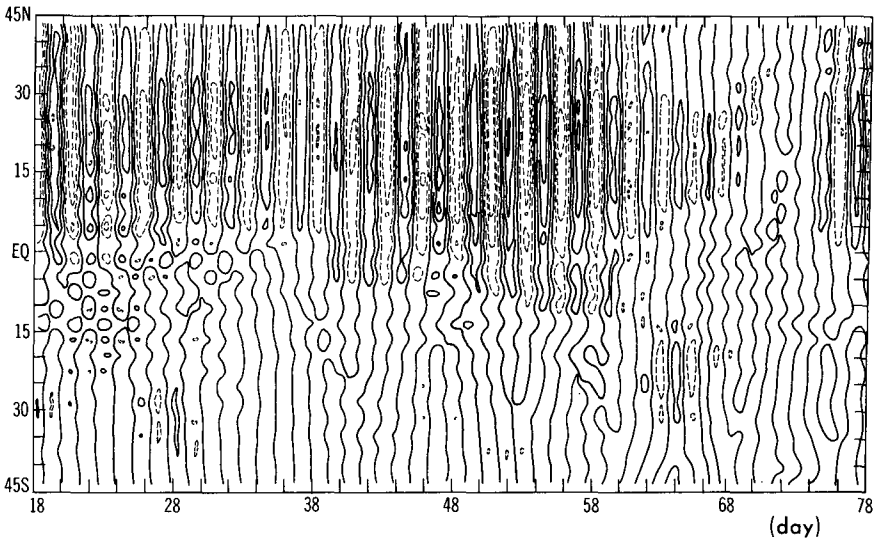

FIG. 21. Time–latitude section of the westward-propagating wavenumber 3 component of 0.2-mb geopotential height at 0° longitude, filtered to retain only periods between 1.9 and 2.6 days. Results for SKYHI during the M1 and M2 periods. Contour interval 5 m.

b. The two-day wave

Many observational studies of transient fluctuations in the mesosphere have found prominent oscillations of about 2-day period, particularly in summer (e.g., Salby 1981b). Salby (1981a,b) identified this 2-day wave with the westward-propagating wavenumber 3 Rossby–gravity normal mode (3,0). Salby (1981a) performed linear calculations of the (3,0) modal structure in a realistic solstitial mean wind configuration. His computations showed that, while in the troposphere the (3,0) mode should retain its basically antisymmetric character, by mesospheric heights the mode should be much intensified in the summer hemisphere (with geopotential amplitude peaking around 25° latitude). This meridional structure has also been found in global satellite observations of the 2-day wave near solstice (Rodgers and Prata 1981).

Figure 21 shows the time–latitude section of the westward-propagating wavenumber 3 component of the 0.2-mb geopotential height resynthesized over the periods ranging from 1.9 to 2.6 days. Results are shown only for SKYHI. The presence of a meridionally coherent wave in the Northern Hemisphere (peaking near 25°N) is apparent over much of the period shown. In the early part of the record (particularly days 18–20 and 26–30) there is some indication of a Southern Hemisphere manifestation of the oscillation that is out of phase with that in the Northern Hemisphere. This overall behavior seems consistent with the expected development of the (3,0) mode during the evolution toward the June solstice. The peak height amplitudes in Fig. 21 of about 10–15 m are very roughly consistent with the observational estimate of temperature amplitudes in the summer hemisphere mesosphere of the order of 0.5 K (Rodgers and Prata 1981). By contrast, nothing recognizable as the (3,0) mode occurs in the corresponding linear model results (not shown).

c. Discussion

Examination of the SKYHI data filtered over frequency ranges characteristic of the Rossby normal modes revealed the clear presence of the (1,1), (1,3), (2,1), and (3,0) modes that are familiar from many earlier observational studies. Amplitudes for these modes appear to be comparable to those seen in observations. There are also indications of the occurrence of the (1,2), (2,2), and (2,3) modes, although these are more difficult to isolate in the limited data produced in the present project.

Some evidence of the occurrence of some of the same Rossby normal modes can be found in the linear model simulation. In all cases, however, the modes in the linear model appear to have at most one-quarter the amplitude seen in the full SKYHI model. Note that the results in section 4 concerning large-scale vertically propagating waves suggest that overall, the dissipation in the linear model is weaker than in SKYHI. Given these findings, it seems clear that latent and convective heating is at most a minor forcing mechanism for the Rossby modes in the SKYHI general circulation model.

A note of caution about the interpretation of the linear model results should be added. Recall that the basic zonal mean flow of SKYHI is modified in the low and middle troposphere at middle and high lati-

tudes, in order to render the linear integration stable (section 3b). This modification may be justified for vertically propagating waves by its negligible influence on the wave activity emanating from the tropical troposphere, but it could influence the Rossby normal modes because of their global nature. However, note that the mean wind modifications employed are typically of the order of 5 m s^{-1}, and so are considerably smaller than the phase speed of the modes.

7. Conclusions

This paper has examined the response of a linear wave model when forced by the parameterized latent and convective heating taken from an integration of the comprehensive SKYHI troposphere–stratosphere–mesosphere GCM. This work is a logical extension of two paths of research that have been pursued over the last two decades: the study of linear wave response to specified idealized tropospheric heating (Holton 1973; Salby and Garcia 1987) and the diagnosis of forcing mechanisms for wave generation using general circulation models experiments (Hayashi and Golder 1978; Hamilton 1987). Practical constraints (particularly on the volume of data that needed to be repeatedly manipulated during analysis) restricted the study to a moderate resolution (3° in latitude), a limited period (78 days), and a reduced meridional domain for analysis (43.5°S–43.5°N). There were also obstacles to constructing an exact linear analog to the full GCM; that is, the nonlinearity of the subgrid-scale dissipation in the GCM and the basic state modification needed to suppress baroclinic instability in the linear model. Despite these limitations, the results presented here are quite striking in some respects, and they lead to some rather unambiguous conclusions.

The SKYHI model was shown to produce a spectrum of eastward-propagating disturbances in the stratosphere dominated by pulses of Kelvin waves with vertical wavelengths and phase speeds similar to the observed Wallace–Kousky wave. At higher altitudes shorter period (longer vertical wavelength) waves dominate, a tendency also seen in observations. For these waves there is an impressive degree of similarity between the linear model and full GCM simulations. The principal difference is a clear tendency for the linear model Kelvin waves to be stronger than those in the SKYHI simulation. These results are consistent with the view that latent and convective heating is the dominant forcing mechanism for these Kelvin waves, and that the effective dissipation of these waves is larger in SKYHI than in the linear model.

The present results on the large-scale eastward waves allow verification of each step in Holton's (1973) scenario for Kelvin wave excitation. The convective heating in the SKYHI troposphere was shown to have a rather broad frequency spectrum (certainly much less monochromatic than the stratospheric response), but with impressive vertical coherence and a vertical extent ~10 km. The resulting stratospheric Kelvin waves all had similar dominant phase speeds and vertical wavelengths, regardless of zonal scale. There is no evidence that wave–CISK plays a role in generating stratospheric Kelvin waves in the model.

The results for global-scale westward-propagating waves contrast strongly with those for the eastward waves. In SKYHI the westward-propagating zonal wavenumbers 1 and 2 are largely explained by Rossby normal modes. The 5-day (1,1), 4-day (2,1), and 16-day (1,3) modes are each clearly identifiable and each appears to have a realistic amplitude. The "2-day wave" is also clearly present in the SKYHI simulation as a westward-propagating global mode. The linear model has at most very weak signals corresponding to the Rossby modes. Thus, in SKYHI at least, tropospheric latent and convective heating is not a major source of excitation for normal modes.

The SKYHI simulation also includes a broad spectrum of shorter-scale, higher-frequency waves. Examination of the EP fluxes associated with these smaller-scale waves suggests that they are largely forced in the low-latitude troposphere, and then spread out into the subtropical and extratropical middle atmosphere. This picture is confirmed to some extent by the linear model results. These show that the equatorial inertia–gravity wave field seen in SKYHI can be adequately explained by the latent and convective heating within a few degrees of the equator. The waves excited by this low-latitude thermal forcing do spread out over a broad meridional range in the stratosphere and mesosphere, but this effect can account for only a fraction of the gravity waves fluxes seen in the SKYHI extratropics.

Acknowledgments. The authors wish to thank Y. Hayashi, J. D. Mahlman, K. Miyakoda, and G. P. Williams for helpful discussions and comments about this work. They also acknowledge the comments of the official reviewers. R. J. Wilson provided assistance with the SKYHI integrations.

REFERENCES

Andrews, D. G., J. D. Mahlman, and R. W. Sinclair, 1983: Eliassen–Palm diagnostics of wave–mean flow interaction in the GFDL SKYHI general circulation model. *J. Atmos. Sci.*, **40**, 2768–2784.

——, J. R. Holton, and C. B. Leovy, 1987: *Middle Atmospheric Dynamics.* Academic Press, 489 pp.

Coy, L., and M. Hitchman, 1984: Kelvin wave packets and flow acceleration: A comparison of modelling and observations. *J. Atmos. Sci.*, **41**, 1875–1880.

Eckermann, S. D., and R. A. Vincent, 1989: Falling sphere observations of anisotropic gravity wave motions in the upper stratosphere over Australia. *Pure Appl. Geophys.*, **130**, 509–532.

Fels, S. B., 1982: A parametrization of scale-dependent radiative damping rates in the middle atmosphere. *J. Atmos. Sci.*, **39**, 1141–1152.

——, 1986: Analytic representations of standard atmosphere temperature profiles. *J. Atmos. Sci.*, **43**, 219–221.

——, J. D. Mahlman, M. D. Schwarzkopf, and R. W. Sinclair, 1980: Stratospheric sensitivity to perturbations in ozone and carbon dioxide: radiative and dynamical response. *J. Atmos. Sci.*, **37**, 2265–2297.

Fritts, D. C., 1984: Gravity wave saturation in the middle atmosphere: A review of theory and observation. *Rev. Geophys. Space Phys.*, **22**, 275–308.

——, and G. D. Nastrom, 1992: Sources of mesoscale variability of gravity waves. Part II: Frontal, convective and jet stream excitation. *J. Atmos. Sci.*, **49**, 111–127.

Garcia, R. R., and J. E. Geisler, 1981: Stochastic forcing of small amplitude oscillations in the stratosphere. *J. Atmos. Sci.*, **38**, 2187–2197.

——, and M. L. Salby, 1987: Transient response to localized episodic heating in the tropics. Part II: Far-field behavior. *J. Atmos. Sci.*, **44**, 499–530.

Hamilton, K., 1987: General circulation model simulation of the structure and energetics of atmospheric normal modes. *Tellus*, **39A**, 435–459.

——, 1988: Evaluation of the gravity wave field in the middle atmosphere of the GFDL SKYHI general circulation model. World Meteorological Organization Technical Document, 273, 264–271.

——, 1991: Climatological statistics of stratospheric inertia-gravity waves deduced from historical rocketsonde wind and temperature data. *J. Geophys. Res.*, **96**, 20 831–20 839.

——, and J. D. Mahlman, 1988: General circulation model simulation of the semiannual oscillation of the tropical middle atmosphere. *J. Atmos. Sci.*, **45**, 3212–3235.

Hayashi, Y., 1970: A theory of large-scale equatorial waves generated by condensation heat and accelerating the zonal wind. *J. Meteor. Soc. Japan*, **48**, 140–160.

——, 1971: A generalized method of resolving disturbances into progressive and retrogressive waves by space Fourier and time cross-spectral analyses. *J. Meteor. Soc. Japan*, **49**, 125–128.

——, and D. G. Golder, 1978: The generation of equatorial transient planetary waves: Control experiments with a GFDL general circulation model. *J. Atmos. Sci.*, **35**, 2068–2082.

——, and ——, 1983: Transient planetary waves simulated by GFDL spectral general circulation models. Part II: Effects of nonlinear energy transfer. *J. Atmos. Sci.*, **40**, 951–957.

——, ——, and J. D. Mahlman, 1984: Stratospheric and mesospheric Kelvin waves simulated by the GFDL SKYHI general circulation model. *J. Atmos. Sci.*, **41**, 1971–1984.

——, ——, ——, and S. Miyahara, 1989: The effect of horizontal resolution on gravity waves simulated by the GFDL SKYHI general circulation model. *Pure Appl. Geophys.*, **130**, 421–443.

Hendon, H. H., and B. Liebmann, 1991: The structure and annual variation of antisymmetric fluctuations of tropical convection and their association with Rossby-gravity waves. *J. Atmos. Sci.*, **48**, 2127–2140.

Hines, C. O., 1960: Internal atmospheric gravity waves at ionospheric heights. *Can. J. Phys.*, **38**, 1441–1481.

Hirooka, T., and I. Hirota, 1985: Normal mode Rossby waves observed in the upper stratosphere. Part II: Second antisymmetric and symmetric modes of zonal wavenumber 1 and 2. *J. Atmos. Sci.*, **42**, 536–548.

Hirota, I., 1978: Equatorial waves in the upper stratosphere and mesosphere in relation to the semiannual oscillation of the zonal wind. *J. Atmos. Sci.*, **35**, 714–722.

——, and T. Hirooka, 1984: Normal mode Rossby waves observed in the upper stratosphere. Part I: First symmetric modes of zonal wavenumber 1 and 2. *J. Atmos. Sci.*, **41**, 1253–1267.

Holton, J. R., 1973: On the frequency distribution of atmospheric Kelvin waves. *J. Atmos. Sci.*, **30**, 499–501.

Kurihara, Y., and J. L. Holloway, Jr., 1967: Numerical integration of a nine-level global primitive equations model formulated by the box method. *Mon. Wea. Rev.*, **95**, 509–530.

Legates, D. R., and C. J. Willmott, 1990: Mean seasonal and spatial variability in gauge-corrected, global precipitation. *Int. J. Climatol.*, **10**, 111–127.

Lindzen, R. S., 1981: Turbulence and stress due to gravity wave breakdown. *J. Geophys. Res.*, **86**, 9707–9714.

Longuet-Higgins, M. S., 1968: The eigenfunctions of Laplace's tidal equation over a sphere. *Philos. Trans. Roy. Soc. London*, **A262**, 511–607.

Madden, R. A., and P. R. Julian, 1972: Description of global-scale circulation cells in the tropics with 40-50 day period. *J. Atmos. Sci.*, **29**, 1109–1123.

Mak, M. K., 1969: Laterally driven stochastic motions in the tropics. *J. Atmos. Sci.*, **26**, 41–64.

Manzini, E., 1992: A numerical study of the middle atmosphere response to tropical and subtropical tropospheric heat sources. Ph.D. dissertation, Princeton University, Princeton, NJ 08544, 173 pp.

Miyahara, S., Y. Hayashi, and J. D. Mahlman, 1986: Interaction between gravity waves and planetary-scale flow simulated by the GFDL SKYHI general circulation model. *J. Atmos. Sci.*, **43**, 1844–1861.

Nastrom, G. D., and D. C. Fritts, 1992: Sources of mesoscale variability of gravity waves. Part I: Topographic excitation. *J. Atmos. Sci.*, **49**, 101–110.

Nitta, T., 1970: Statistical study of tropospheric wave disturbances in the tropical Pacific region. *J. Meteor. Soc. Japan*, **48**, 47–60.

Rodgers, C. D., and A. J. Prata, 1981: Evidence for a traveling two day wave in the middle atmosphere. *J. Geophys. Res.*, **86**, 9661–9664.

Salby, M. L., 1981a: Rossby normal modes in nonuniform background configurations. Part II: Equinox and solstice conditions. *J. Atmos. Sci.*, **38**, 1827–1840.

——, 1981b: The 2-day wave in the middle atmosphere: Observations and theory. *J. Geophys. Res.*, **86**, 9654–9660.

——, 1984: Survey of planetary-scale travelling waves: The state of theory and observations. *Rev. Geophys. Space Phys.*, **22**, 209–236.

——, and R. R. Garcia, 1987: Transient response to localized episodic heating in the tropics, Part I: Excitation and short-time near-field behavior. *J. Atmos. Sci.*, **44**, 458–498.

——, D. L. Hartmann, and J. C. Gille, 1984: Evidence for equatorial Kelvin modes in *Nimbus-7* LIMS. *J. Atmos. Sci.*, **41**, 220–235.

Taylor, R. C., 1973: An atlas of Pacific island rainfall. Hawaii Institute of Geophysics Report, University of Hawaii, Honolulu, Hilo, HI 96720.

Vincent, R. A., and D. C. Fritts, 1987: A climatology of gravity wave motions in the mesosphere at Adelaide, Australia. *J. Atmos. Sci.*, **44**, 748–760.

Wallace, J. M., 1973: General circulation of the tropical lower stratosphere. *Rev. Geophys. Space Phys.*, **11**, 191–222.

——, and V. E. Kousky, 1968: Observational evidence of Kelvin waves in the tropical stratosphere. *J. Atmos. Sci.*, **25**, 900–907.

Yanai, M., and T. Maruyama, 1966: Stratospheric wave disturbances propagating over the equatorial pacific. *J. Meteor. Soc. Japan*, **44**, 291–293.